AD-A250 282

(2)

SECURITY

DOCUMENTATION PAGE

1a. REPORT SECURITY CLASSIFICATION: UNCLASSIFIED	1b. RESTRICTIVE MARKINGS: NONE
2a. SECURITY CLASSIFICATION AUTHORITY	3. DISTRIBUTION/AVAILABILITY OF REPORT: UNLIMITED. This document has been approved for public release and sale; its distribution is unlimited.
2b. DECLASSIFICATION/DOWNGRADING SCHEDULE	
4. PERFORMING ORGANIZATION REPORT NUMBER(S)	5. MONITORING ORGANIZATION REPORT NUMBER(S): AFOSR-TR- 92 0387
6a. NAME OF PERFORMING ORGANIZATION: Dept. of Mechanical, Aeronautical and Materials Engineering, University of California	6b. OFFICE SYMBOL (If applicable)
6c. ADDRESS (City, State, and ZIP Code): Davis, CA 95616-5294	7a. NAME OF MONITORING ORGANIZATION: Same as 8c
	7b. ADDRESS (City, State, and ZIP Code): Same as 8c
8a. NAME OF FUNDING/SPONSORING ORGANIZATION: AFOSR	8b. OFFICE SYMBOL (If applicable): NC
	9. PROCUREMENT INSTRUMENT IDENTIFICATION NUMBER: AFOSR-89-0287
8c. ADDRESS (City, State, and ZIP Code): Dr. Alan H. Rosenstein, AFOSR/NC, Building 410, Bolling Air Force Base, DC 20332-6448	10. SOURCE OF FUNDING NUMBERS: PROGRAM ELEMENT NO. 61102F; PROJECT NO. 2306; TASK NO. AS; WORK UNIT ACCESSION NO. -

11. TITLE (Include Security Classification)
(u) Strengthening Mechanisms, Creep and Fatigue Processes in Dispersion Hardened Niobium Alloy.

12. PERSONAL AUTHOR(S) AMIYA K. MUKHERJEE & JEFFERY C. GIBELING

13a. TYPE OF REPORT	13b. TIME COVERED	14. DATE OF REPORT (Year, Month, Day)	15. PAGE COUNT
Final Scientific Report	FROM 2/1/89 TO 1/31/92	April 20, 1992	56

16. SUPPLEMENTARY NOTATION

17. COSATI CODES			18. SUBJECT TERMS (Continue on reverse if necessary and identify by block number)
FIELD	GROUP	SUB-GROUP	Keywords: creep, fatigue, niobium alloy, dislocation mechanisms
11.06			

19. ABSTRACT (Continue on reverse if necessary and identify by block number)

The creep and fatigue properties of pure Nb and Nb-1%Zr alloy were investigated. A model was developed based on the migration of subgrain boundary that can explain the "anomalous" primary creep transients found in Nb-1%Zr alloy, due to coarsening of subgrain structure. TEM investigations confirmed that such subgrain coarsening occurs during primary creep of Nb-1%Zr. Baseline low cycle fatigue studies of Nb and Nb-1%Zr were completed. Cyclic hardening is observed and there is a microplastic plateau in Nb. The Nb-1%Zr is stronger in cyclic deformation than Nb, with little influence of strain rate. The deformation in the alloy at both high and low strain rates is controlled by the interaction between gliding edge dislocation and solute atoms.

20. DISTRIBUTION/AVAILABILITY OF ABSTRACT	21. ABSTRACT SECURITY CLASSIFICATION	
☒ UNCLASSIFIED/UNLIMITED ☐ SAME AS RPT. ☐ DTIC USERS	UNCLASSIFIED	
22a. NAME OF RESPONSIBLE INDIVIDUAL: Alan H. Rosenstein	22b. TELEPHONE (Include Area Code): (202) 767-4960	22c. OFFICE SYMBOL: AFOSR/NC

DD FORM 1473, 84 MAR — 83 APR edition may be used until exhausted. All other editions are obsolete. — SECURITY CLASSIFICATION OF THIS PAGE

FINAL TECHNICAL REPORT

for

Grant No. AFOSR 89-0287

for the period

February 1, 1989 to January 31, 1992

Strengthening Mechanisms, Creep and Fatigue Processes in Dispersion Hardened Niobium Alloy

submitted to:

AFOSR/NC
Building 410
Bolling Air Force Base, D.C. 20332-6448
Attention: Dr. Alan H. Rosenstein

submitted by:

Professors Amiya K. Mukherjee and Jeffery C. Gibeling
Division of Materials Science and Engineering
Department of Mechanical, Aeronautical and Materials Engineering
University of California, Davis, CA 95616

April 1, 1992

Contents

1 INTRODUCTION

The focus of this research program is on the development and characterization of refractory metals for advanced aerospace structural applications at elevated temperatures. These applications include nuclear space power reactors and hypersonic vehicles such as the National Aerospace Plane (NASP). Systems such as these will involve static loading at elevated temperatures as well as cyclic loading imposed by large thermally induced strains. As a consequence, the creep and low cycle fatigue behavior will be critical material properties in these designs. Compared to alternative candidate materials sytems such as titanium aluminide composites, carbon–carbon composites and ceramic matrix composites, the refractory metals offer substantially better ductility and easier formability. Niobium has been chosen because it has the lowest density among the refractory metals, although its strength at elevated temperatures is well below the desired design goals. The focus of our work to improve the strength of this material is on the influence of dispersed, inert ceramic particles on the creep and low cycle fatigue behavior of niobium. Our specific investigation involves studies of the kinetics of internal oxidation and nitridation of Nb–1%Zr and the creep and low cycle fatigue behavior of dispersion strengthened niobium. The introduction of dispersoids provides an attractive alternative to other strengthening methods such as solid solution stengthening, which is not effective at the temperatures of interest, and fiber reinforcing, which is limited by interfacial reactions between the matrix and the fibers. The work of this program provides the necessary fundamental understanding of the creep and fatigue of the base materials (without dispersoids) to support future basic studies of dispersion strengthened niobium.

During the three years of this program the creep studies have focussed on the behavior of RRR - grade pure niobium, commercially pure (cp) Nb–1%Zr and RRR - grade pure (RRR) Nb–1%Zr. RRR is the terminology used by the supplier to specify high purity niobium and Nb–1%Zr, respectively. Thorough transmission electron microscope (TEM) investigations have shown that in the as–received condition the material contains only a few particles. Efforts to improve the creep strength by internal oxidation or nitridation have failed due to the rapid coarsening of the particles which causes a decrease in the creep strength. Our main focus was therefore to explain the "anomalous" primary creep transients on the basis of subgrain coarsening. Based on this model, which received support from TEM – investigations, we were able to describe and model the creep behavior of RRR grade Nb–1%Zr. Furthermore this material can be considered as a model material due to the absence of particles and carbides. The results obtained on this material are extremely useful in explaining the primary creep behavior of particle and/or dispersion hardened materials.

During the same period, we have completed a fundamental study of the mechanisms of low cycle fatigue in commercially pure niobium (cp Nb) and the Nb–1%Zr alloy. Both materials were tested at plastic strain amplitudes in the range $0.02\ \% \leq \Delta\epsilon/2 \leq 0.7\ \%$. At low temperatures, the cyclic deformation response of BCC metals is strongly dependent on strain

rate. Thus, it was necessary to test at slow ($2 \cdot 10^{-4}s^{-1}$) and fast ($2 \cdot 10^{-2}s^{-1}$) strain rates in order to fully characterize the cyclic deformation. Only cyclic hardening was observed for both metals under all testing conditions. As expected, higher cyclic stresses were recorded at the fast strain rate compared to the slow strain rate. The Nb–1%Zr alloy was always stronger than cp Nb, although both metals had the same cyclic life at equal plastic strain amplitudes. Further, the strain rate had no effect on the cyclic life. At the fast strain rate intergranular cracking occurred and a microplastic plateau was observed in the cyclic stress – strain curve for cp Nb. At the slow strain rate, no definitely intergranular cracks were detected and a microplastic plateau was not observed for cp Nb. The results of these experiments can be interpreted in terms of the influence of strain rate and solute content on the relative mobilities of edge and screw dislocations.

2 RESEARCH HIGHLIGHTS

During the three years of our program, we have:

1. Developed the equipment, software and procedures to conduct monotonic and high resolution stress change tests at temperatures up to 1300 K in vacuum and low cycle fatigue tests at various strain rates;

2. Measured the monotonic creep properties of RRR grade pure niobium, cp Nb–1%Zr and RRR Nb–1%Zr. As received materials were used containing only a few dispersoids. Efforts to improve the creep strength by internally oxidizing or nitriding have failed due to the coarsening of the formed particles that resulted in a weakening of the creep strength;

3. Developed a model based on the migration of subgrain boundary migration that can explain the "anomalous" primary creep transients found in Nb–1%Zr by coarsening of the subgrain structure;

4. Conducted thorough TEM investigations which confirm that subgrain coarsening occurs during primary creep of Nb–1%Zr;

5. Completed the baseline low cycle fatigue studies of commercially pure polycrystalline Nb and Nb-1Zr. We have used low strain rates to determine high temperature behavior and high strain rate to assess low temperature characteristics. Cyclic hardening is observed and there is a microplastic plateau in the pure Nb. In addition, the effect of strain rate suggests that deformation of the pure Nb is controlled by the Peierls stress acting on gliding screw dislocations;

6. Shown that Nb–1%Zr is stronger in cyclic deformation than Nb, with little influence of strain rate. Deformation at both strain rates is controlled by the interaction between gliding edge dislocations and solute atoms;

7. Analyzed the hysteresis loop data from low cycle fatigue tests to show that even when the applied stress remains constant (in saturation), microstructural changes lead to variations in the backstress and friction stress components.

3 MATERIALS AND EXPERIMENTAL PROCEDURES

3.1 Materials

3.1.1 Composition and manufacturing

In the present work four different kind of materials have been used:
RRR – grade niobium, cp Nb–1%Zr, RRR Nb–1%Zr. The chemical composition of the three materials is given in the appendix A. The niobium and niobium alloys that are being used in this study were supplied by Teledyne Wah Chang in Albany, Oregon. The materials were processed by compacting powder, arc melting, machining, forging, and rolling sheet (for creep samples) or extruding rod (for the fatigue samples). The sheets were given a two hour annealing treatment at 1477 K after the final rolling operation, whereas the rods were annealed for 1 hour at 1473 K. We note that these annealing treatments are not adequate to ensure complete recrystallization. For further details about the manufacturing process, the heat treatment, and the impurity content see appendix A.

3.1.2 Material parameters

Niobium and Nb–1%Zr have a body centered cubic (bcc) crystal structure. The following table lists some material parameters for pure niobium:
(The values were taken from Frost and Ashby [13])

Atomic volume (m^3)	Ω	=	$1.80 \cdot 10^{-29}$
Burgers vector (m)	b	=	$2.86 \cdot 10^{-10}$
Melting temperature (K)	T_M	=	2741
Shear modulus (GPa)	G	=	44.3
Temp. dep. of G	$\frac{\partial G}{\partial T}$	=	0.0
Activation energy (kJ/mole) (Lattice diffusion)	Q_v	=	401

According to Frost and Ashby there is no temperature dependence of the shear modulus. This is hard to believe. Our own literature research revealed that there is a "wide range" of G – values available. Due to these uncertainties we decided to take as a maximum value for G for Nb–1%Zr the value from Frost and Ashby, and as a minimum value 21.4 GPa derived from our own creep tests.

3.2 Creep testing

3.2.1 Sample preparation

Tensile specimens were punched from 1mm thick cp Nb–1%Zr sheet using a custom made punch and die set. Samples from the RRR Nb and RRR Nb–1%Zr sheets were prepared by machining. Tensile specimens parallel to the rolling direction as well as perpendicular to the rolling direction were prepared to examine the influence of texture. All samples were tested without further heat treatment, except in the few cases noted. Prior to testing all samples were wrapped in niobium foil to prevent oxidation during the creep tests due to the residual oxygen in the retort of the vacuum creep machine. In figure 1 a set of tensile specimens is shown.

The grain size of the different materials prior to deformation was:

material	*grain size in μm*
RRR Nb	12 ± 3
cp Nb–1%Zr	14 ± 6
RRR Nb–1%Zr	16 ± 8

Table 1: Grain size of the three materials used

The grains were equiaxed. No texture was visible. The difference in the grain sizes was explained by different processing by the manufacturer.

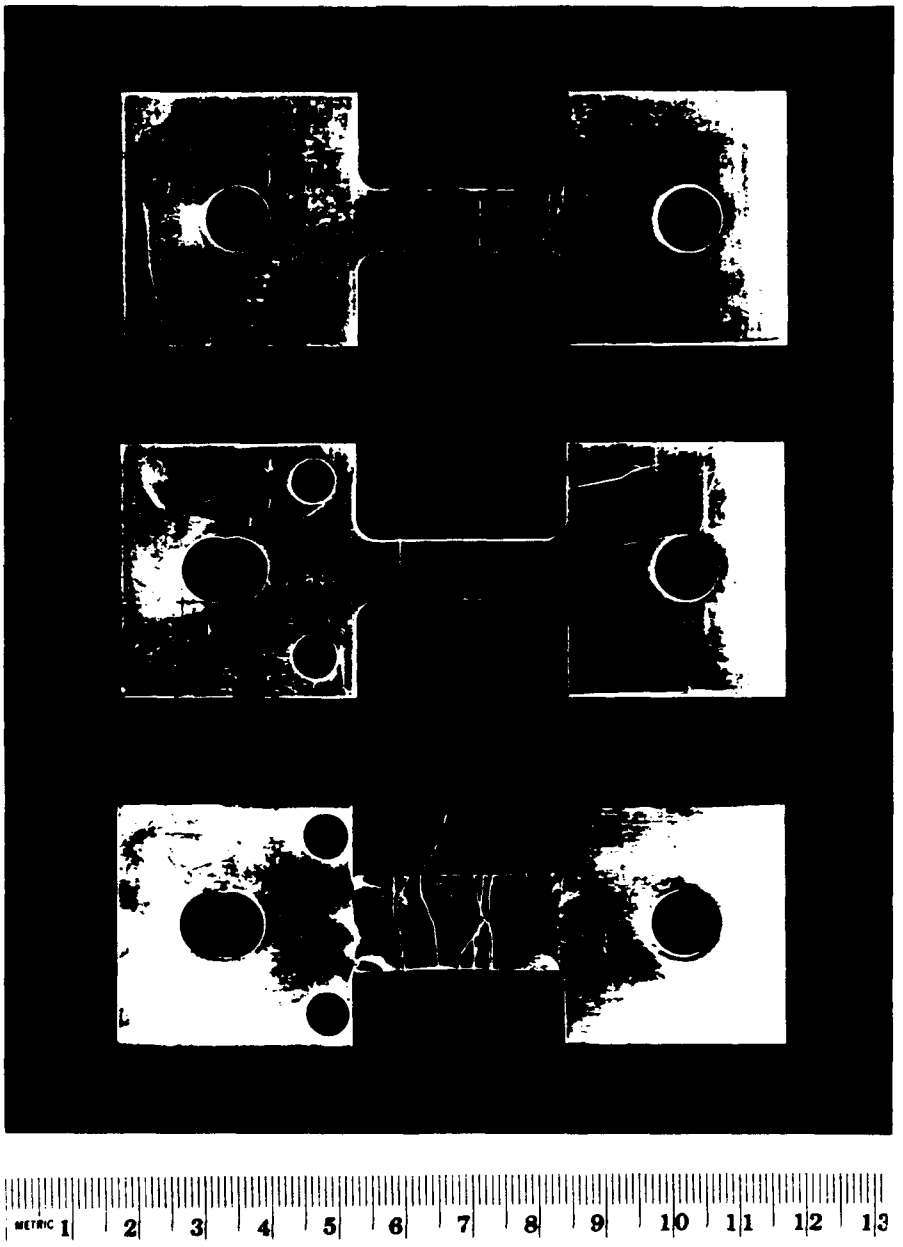

Figure 1: a) Specimen after punching or machining, b) modified shape of the specimen, and c) sample wrapped in niobium foil. For further details see section 3.2.2

3.2.2 Test equipment

The creep tests were performed in an apparatus purchased from Applied Test Systems (ATS) with funding obtained from a previous AFOSR equipment grant. The creep apparatus together with Andrade Chalmers lever arm for constant stress experiments in tension, retort, furnace, temperature control unit, and vacuum system is shown in figure 2 on page 10. In order to conduct creep tests at elevated temperatures some modifications to the creep set up were necessary:

1. A vacuum system was attached to the creep machine in order to prevent the samples from becoming oxidized;
2. Water cooling for the SLVC was installed in order to prevent the transducer from overheating during the creep tests. (The SLVC is inside the retort);
3. The linkage was modified in order to be able to measure only the deformation of the gage section;
4. A load cell was mounted in the load train to directly measure the load acting on the sample;
5. A personal computer and a 16 bit A/D converter were purchased to monitor the creep tests with a high time and strain resolution.

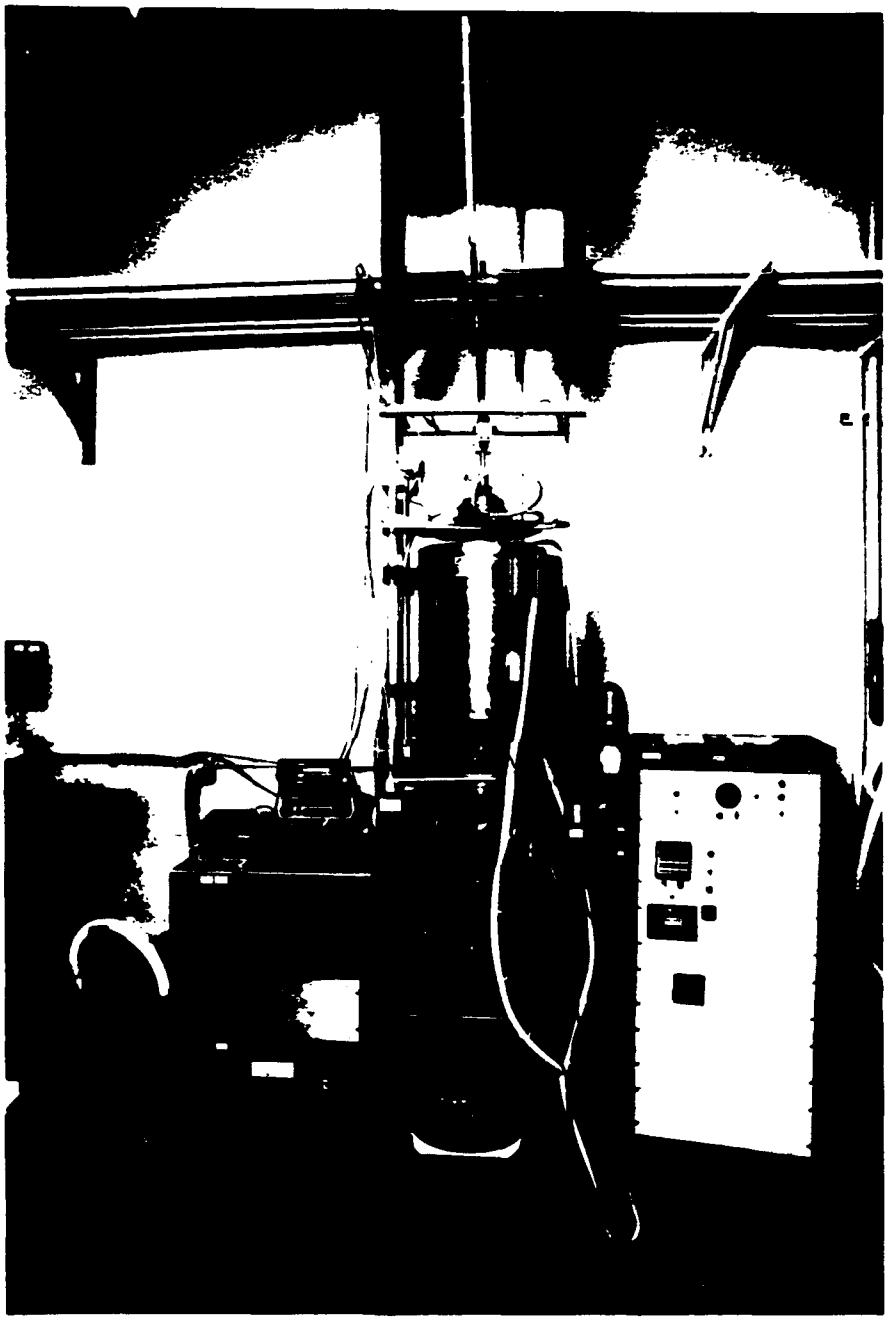

Figure 2: Creep testing equipment

To heat the samples to test temperatures of 1200 K and 1300 K, respectively, a single zone resistance furnace was used. The time necessary for heating up was usually in the range of 90 min. In order to expose the samples to the same heat treatment, a heating time of 120 min was applied to every sample. All test were done in vacuum at pressures ranging from $2 \cdot 10^{-3}$ Pa to $6.6 \cdot 10^{-4}$ Pa. The deformation of the samples was measured with a Super Linear Variable Capacitor (SLVC) which has a resolution of $2.54 \cdot 10^{-5}$ mm. The force acting on the specimen was measured with a load cell which was mounted directly in the load train. The two signals, force and displacement, were sent to an 16 bit A/D – converter and from this to a personal computer. With this system, it is possible to measure (true) strains up to 54% with a strain resolution of approximately $1 \cdot 10^{-5}$ and a time resolution of up to 100 μs.

3.2.3 Test methods

Two different test methods were used to monitor the deformation behavior of pure niobium and the niobium alloys:
Normal Mode:
Normal mode with an acquisition rate of 10 sets of data points per 0.35 s was used while recording monotonic creep tests. The storage of data points was controlled either by a variable strain or time criterion.

Fast Mode:
Fast mode was used while recording the transient behavior after stress reductions of variable amounts. Shortly before the stress reduction, or the so–called dip test, data acquisition was switched from the normal to the fast mode with acquisition rates of up to 10 kHz. After an adjustable time span the data acquisition program automatically switched back to normal mode. The fast mode was very helpful in measuring the response of a material to sudden change in stress, where the main emphasis is in the events shortly after the stress drop, usually in a time range of 1 to 2 s.

3.3 LCF testing

3.3.1 Specimen description and preparation

The specimens had a diameter of 6.35 mm and a uniform gage length of 10.2 mm; figure 3 shows the specimen shape and dimensions. The specimens were machined with the gage length having a maximum 0.81 micron RMS finish. After machining, the specimens were successively ground and polished on a lathe using 600 grit sandpaper, then six micron and one micron diamond paste. The specimens were tested without further heat treatment.

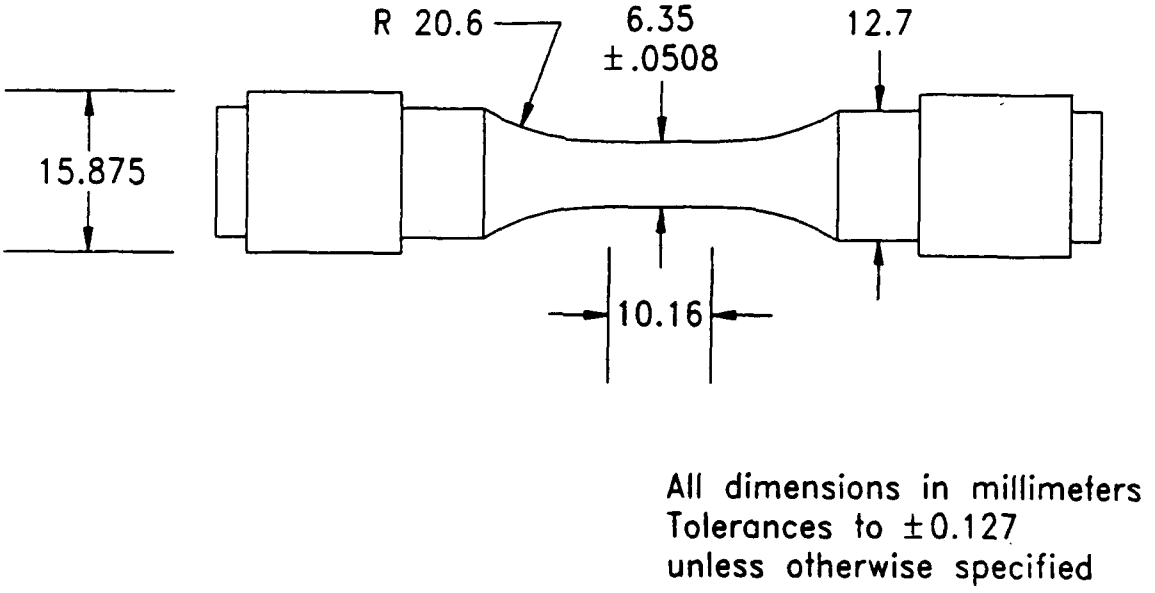

Figure 3: Low cycle fatigue specimen dimensions

3.3.2 Test procedures

The cyclic deformation tests were conducted using a fully automated, closed loop servohydraulic materials test system purchased with funds obtained from a prior AFOSR equipment grant. The strain was measured with a 7.6 mm gage length extensometer attached to the specimen with rubber bands. Initially, 90 degree extensometer knife edges, with a 0.05 mm edge radius of curvature, were used. However, the knife edges created fairly deep impressions in the soft cp Nb material, resulting in crack initiation at the indentations. To minimize this problem 180 degree blunt knife edges were used for all subsequent tests. The specimens were held by mechanical grips of a split collet design. The axis of the specimen was aligned to within 0.013 mm of the actuator axis during installation.

Typically, a low cycle fatigue specimen is fully reverse loaded such that the magnitude of the negative strain equals the magnitude of the positive strain. The controlled variable is usually the total strain amplitude. However, since the material response is determined by the plastic strain, the present experiments were conducted using plastic strain amplitude as the controlled variable. The test command signal was saw-toothed (or triangular) in shape. For each individual test, the machine was programmed to maintain a constant total strain rate. However, as outlined below, to achieve a constant average plastic strain rate (at either the fast or slow strain rate), the total strain rate varied with the plastic strain amplitude of the test.

All tests were conducted at room temperature. Both metals were tested at both slow and fast plastic strain rates of $2 \cdot 10^{-4}s^{-1}$ and $2 \cdot 10^{-2}s^{-1}$. For a given strain rate (slow or fast), the average plastic strain rate was maintained constant. This rate is defined by the following equation 1:

$$\dot{\epsilon}_{pl} = 2\,\nu\,\Delta\epsilon_{pl} \tag{1}$$

where $\dot{\epsilon}_{pl}$ is the average plastic strain rate, ν is the frequency, and $\Delta\epsilon_{pl}$ is the plastic strain range. Given a plastic strain rate and a plastic strain amplitude, the appropriate test frequency was calculated using Equation 1. The total strain rate used in the test machine program was determined from the frequency, the plastic strain amplitude and the elastic strain amplitude estimated from the monotonic data.

Load and strain outputs from the testing machine were converted to digital data pairs by simultaneously triggering two Hewlett Packard 3457 digital multimeters. The data pairs were sent to a personal computer for storage and calculation of the outer (plastic strain) loop control parameters. Data were stored in sets of 200 or 400 data pairs that defined individual hysteresis loops.

At the slow strain rate real-time computer control was possible. As each load and total strain data pair was obtained, the plastic strain was calculated from these two values; if the desired amplitude had been reached or exceeded, a control signal reversed the loading direction. At the fast strain rate, this mode of real-time control was not possible. Instead, the programmable function generator was used to control the total strain amplitude. Sets of 200 load- strain data pairs corresponding to one or two complete hysteresis loops were acquired and analyzed by the control software to determine the actual plastic strain amplitude. A corrected total strain amplitude setting was then sent to the function generator in order to achieve the desired plastic strain amplitude.

3.4 Characterization

3.4.1 Optical Microscopy

In order to prepare the samples for optical microscopy the following steps were necessary:

1. Cutting the samples with a diamond saw
2. Manually grinding to a thickness of 150 μm on both sides equally
3. Polishing with a Buehler Minimet to a thickness of 50 to 100 μm
4. Ion milling

3.4.2 Transmission Electron Microscopy

In Appendix A the procedures for TEM sample preparation are listed.

3.5 Error calculations

The errors and errorbars given together with the values grain size, subgrain size and dislocation density were derived from the following equation:

$$\Delta M = \Delta\sigma \cdot t_{0.05}/\sqrt{n} \tag{2}$$

where M is the measured value, $\Delta\sigma$ the standard deviation, t the security factor derived from the student distribution at a confidence interval of 95% and, n the number of occurences.

4 CREEP TEST RESULTS AND DISCUSSION

4.1 Constant stress experiments

Most of the creep tests were performed on samples prepared perpendicular to the rolling direction at temperatures of 1200 K and 1300 K. A comparison of the creep rates, however, between samples prepared parallel and perpendicular to the rolling direction is also presented.

4.1.1 Dislocation structure

The following figure shows the subgrain size w and the dislocation spacing $\rho_i^{-0.5}$ within subgrains as a function of the shear modulus normalized stress σ for pure niobium. Plotted are data from various authors (Brinson and Argent [11], Vandervoort [17], Arndt [1] and Davidson et al. [12]). Blum, Absenger and Feilhauer [5] pointed out that it is a well established observation that during steady state creep of pure FCC metals the subgrain size w and and the dislocatior spacing in the subgrain interior, $\rho_i^{-0.5}$, are detremined by σ/G. From figure 4 it can be seen that the relations

$$w/b = \beta\,(\sigma/G)^{-1} \tag{3}$$

$$\rho_i^{-0.5} = \alpha\,M\,(\sigma/G)^{-1} \tag{4}$$

also hold for pure niobium. In the above equations b is the Burgers vector, α and β are constants and M the Taylor factor. By inserting ≈ 1 for α, 48 for β and 2.75 for the Taylor factor, one obtains a good agreement with the measured values (dotted lines).

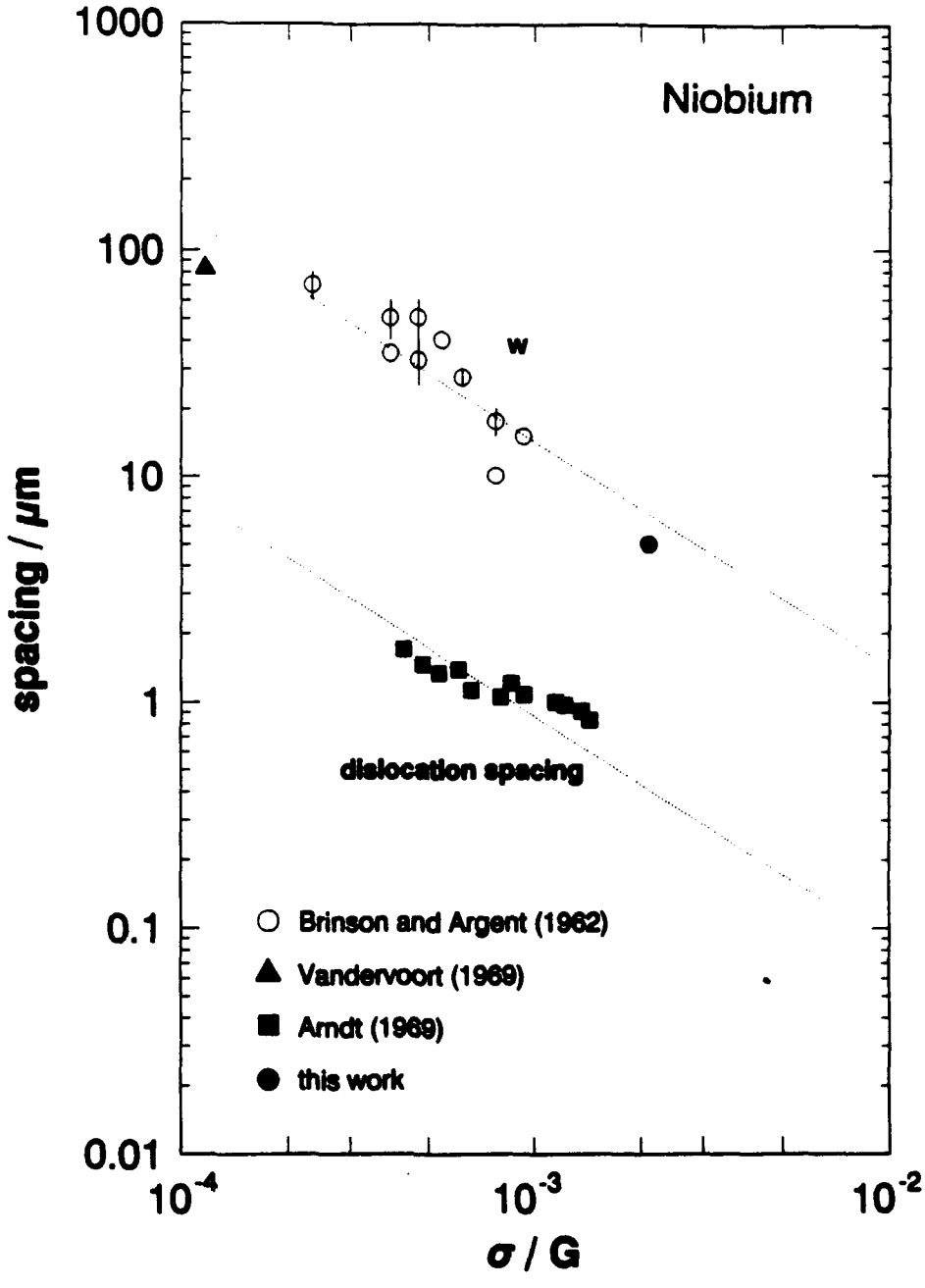

Figure 4: Subgrain size w and dislocation spacing $\rho_i^{-0.5}$ within subgrain as a function of the shear modulus normalized stress σ for pure niobium

4.1.2 Creep rate as a function of strain

On the pages 17 to 19 sets of creep curves for RRR grade Nb tested at 1300 K, cp Nb–1%Zr tested at 1300 K, RRR grade Nb–1%Zr tested at 1300 K parallel and perpendicular to the rolling direction and RRR grade Nb–1%Zr tested at 1200 K are shown.

In these figures, the data are plotted as creep $\dot{\epsilon}$ as a function of (true) creep strain ϵ. It is more suitable to plot the data in this manner than in the usual strain – time plots, because the steady state or minimum creep rates show up more clearly.

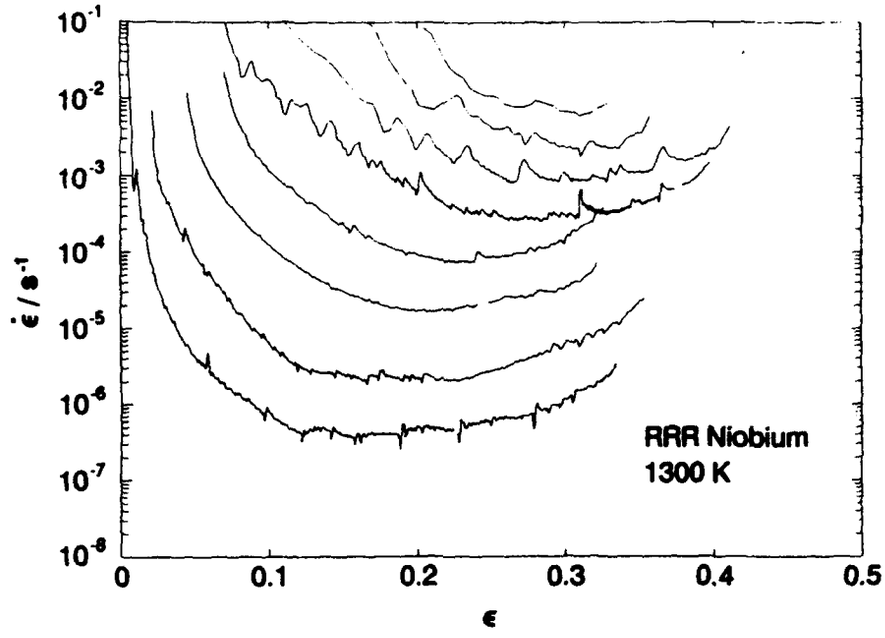

Figure 5: Creep rate $\dot{\epsilon}$ as a function of strain ϵ for RRR grade niobium at 1300 K and various stresses (samples prepared perpendicular to the rolling direction)

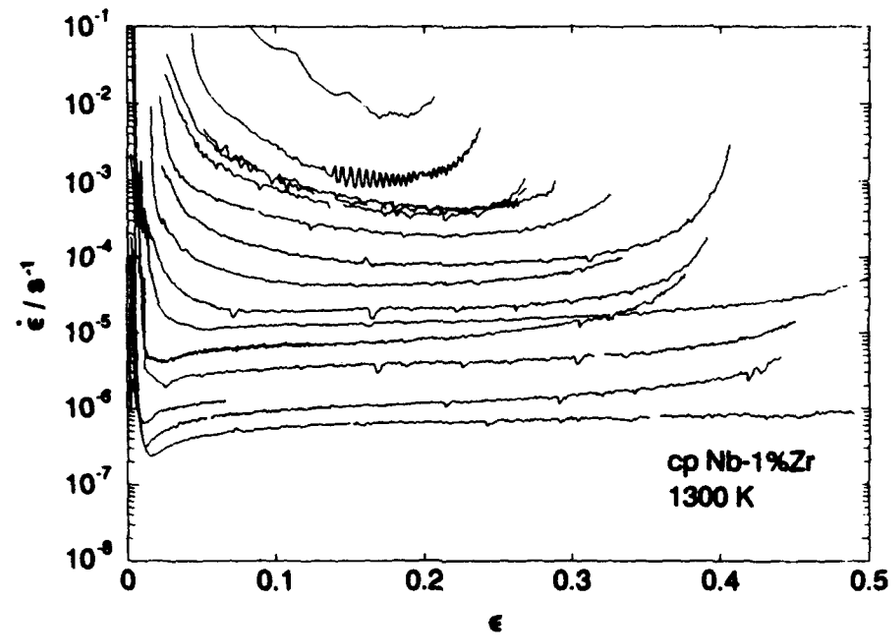

Figure 6: Creep rate $\dot{\epsilon}$ as a function of strain ϵ for cp Nb–1%Zr at 1300 K and various stresses (samples prepared perpendicular to the rolling direction)

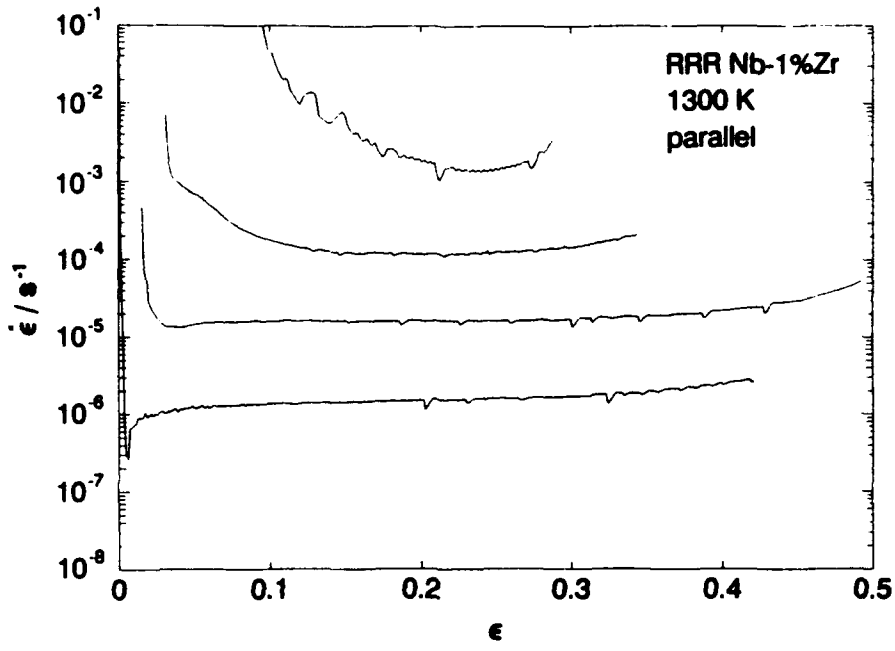

Figure 7: Creep rate $\dot{\epsilon}$ as a function of strain ϵ for RRR grade Nb–1%Zr at 1300 K and various stresses. Samples were prepared parallel to the rolling direction

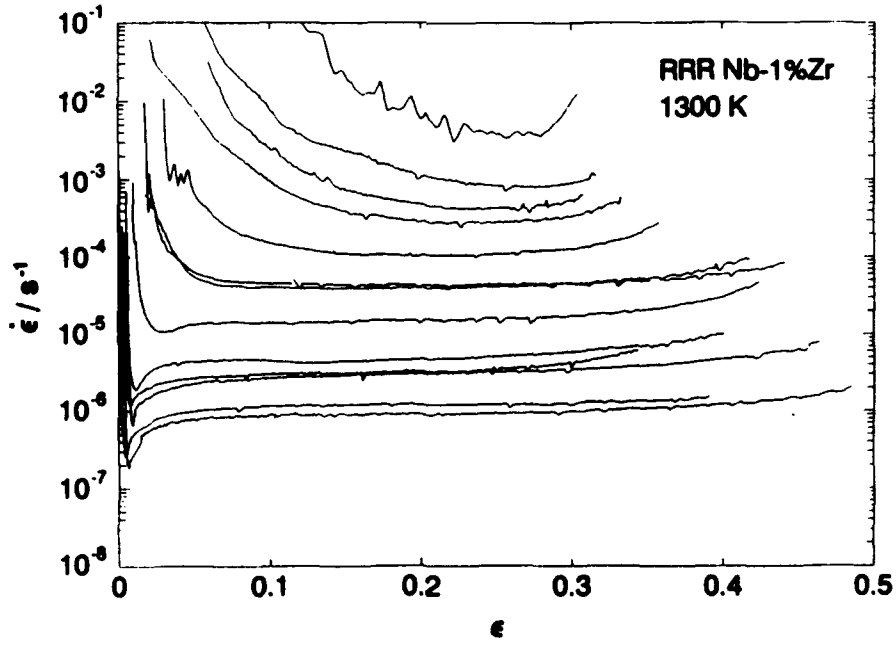

Figure 8: Creep rate $\dot{\epsilon}$ as a function of strain ϵ for RRR grade Nb–1%Zr at 1300 K and various stresses (samples prepared perpendicular to the rolling direction)

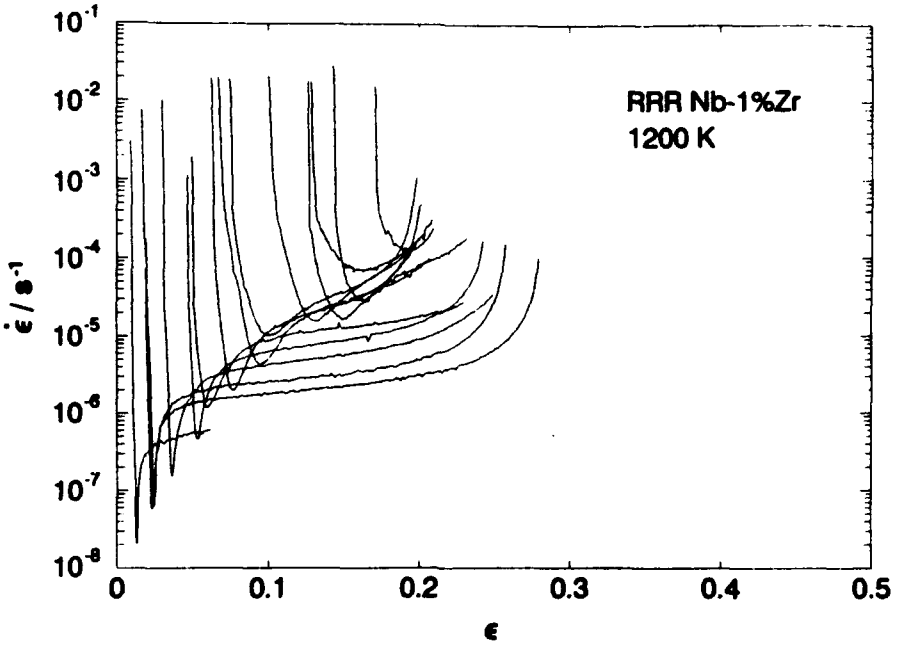

Figure 9: Creep rate $\dot{\epsilon}$ as a function of strain ϵ for RRR grade Nb–1%Zr at 1200 K and various stresses (samples prepared perpendicular to the rolling direction)

According to the results shown in figures 5 to 9, the creep behavior of the various materials is different. The following observations summarize the major differences:

RRR niobium at 1300 K:

Independent of the stress, the creep rates decrease after loading. These so–called "primary creep transients" are very typical transients for a pure material where during primary transient creep the dislocation density in the subgrain interior increases, the internal forward stresses increase, a network of subgrain boundaries starts to form and therefore the creep rates decrease. Following the primary transients a more or less pronounced steady state region can be observed in which an equilibrium between work hardening and recovery exists. As a consequence, the creep rate remains fairly constant. After further straining the so–called region III of creep is reached where an increase in the creep rate can be observed. This increase is due to the formation and/or growth of vacancies and interlinkage of cavities which finally lead to the catastrophic failure of the the sample.

cp Nb–1%Zr at 1300 K, RRR Nb–1%Zr at 1300 K and 1200 K

The creep behavior of cp Nb–1%Zr at 1300 K and RRR Nb–1%Zr at 1300 K (tested parallel and perpendicular to the rolling direction) is different from pure niobium. These materials also exhibit "normal" primary creep transients, but only at high stresses. At lower stresses, the creep rate decreases until a minimum is reached. This minimum becomes more pronounced and sharper the lower the applied stress is. It also tends to shift towards lower strains with deceasing stress. After the minimum, the creep rate accelerates to a plateau with a constant

creep rate until region III is entered where failure of the sample occurs. With the exception of the long range of steady state creep such behavior could be attributed to a material containing particles that coarsen during creep. In those instances, however, a plateau region is generally not observed (compare Blum and Reppich [7]).

A comparison between figs. 7 and 8, i.e. creep curves obtained from samples prepared parallel and perpendicular to the rolling direction, respectively, reveals no significant differences. We conclude that an influence of texture can be neglected.

In figure 9 creep curves for RRR Nb–1%Zr tested at 1200 K are plotted. There is no qualitative difference between the results obtained at 1200 K and 1300 K. However, the overall strains that can be obtained are shorter due to the lower temperatures. Also a so–called "loading" strain can be observed, which is due to the high stresses that cause a "free flight" of individual dislocation resulting in instantaneous strains which depend on the level of the stress.

The minimum creep rates were depicted from creep curves which exhibit a minimum. The steady state creep rates were depicted from the horizontal or plateau like region in the case of RRR Nb–1%Zr at 1300 K and at the inflection point (after the minimum) in the case of RRR Nb–1%Zr at 1200 K.

4.1.3 Creep rate as a function of stress

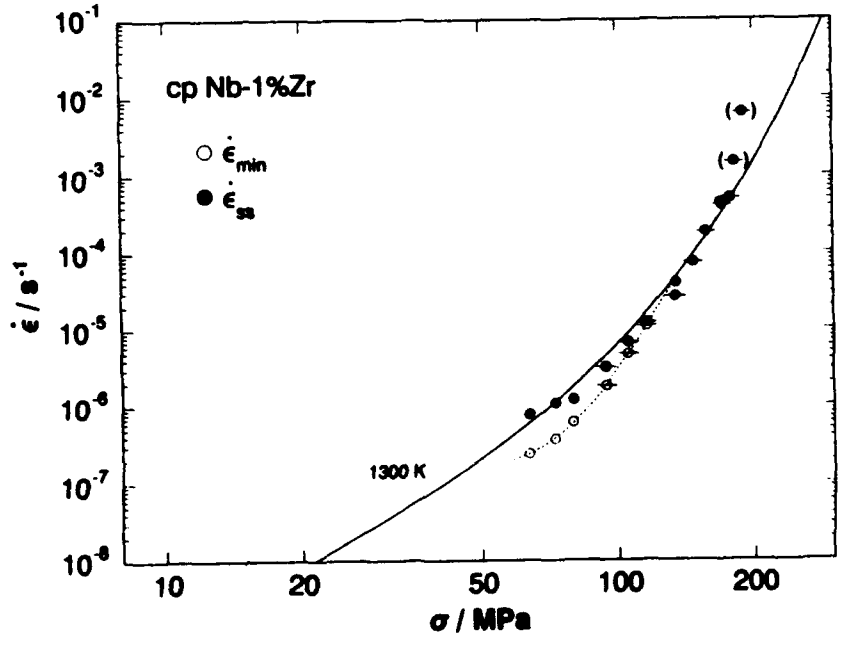

Figure 10: Creep rate $\dot{\epsilon}$ as a function of stress σ for cp Nb–1%Zr at 1300 K

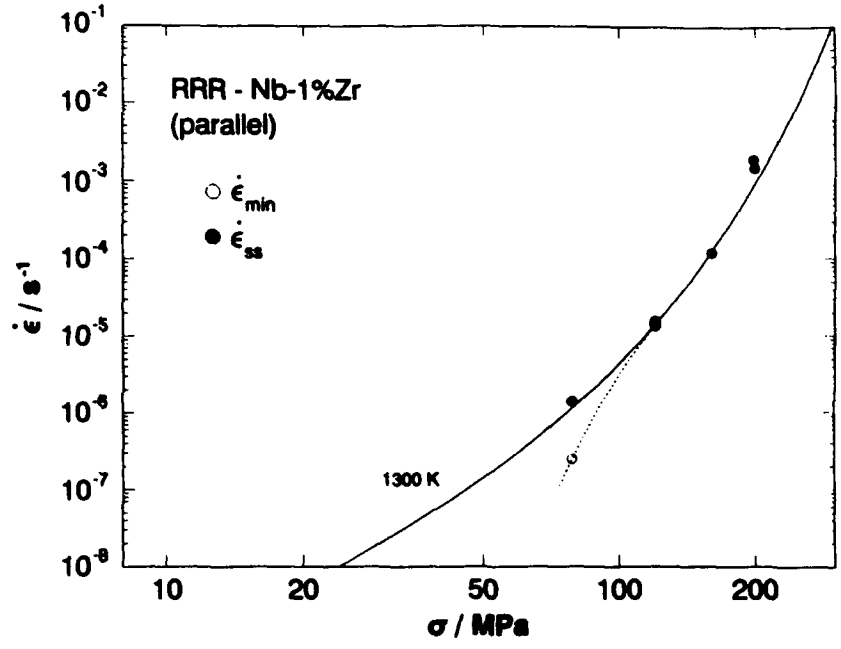

Figure 11: Creep rate $\dot{\epsilon}$ as a function of stress σ for RRR Nb–1%Zr at 1300 K (parallel to the rolling direction)

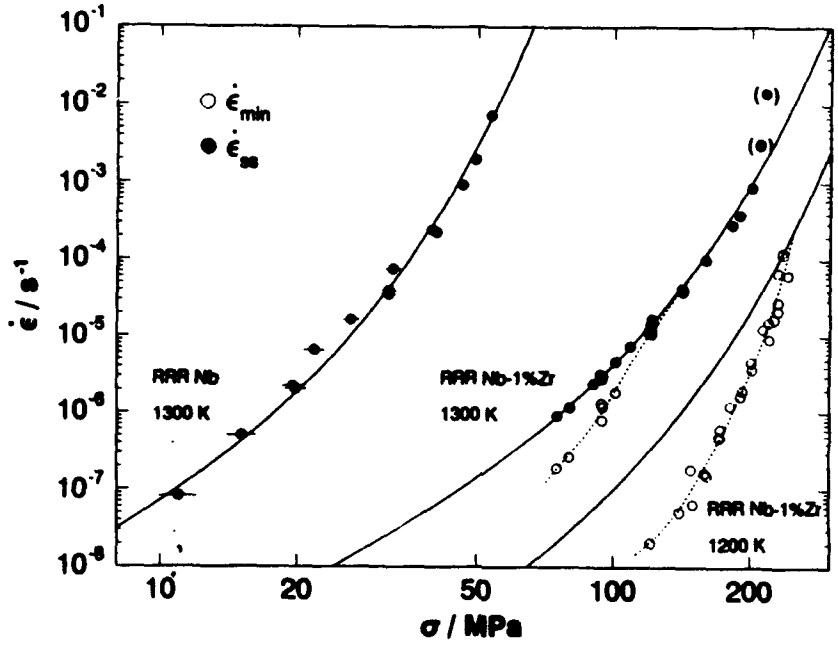

Figure 12: Creep rate $\dot{\epsilon}$ as a function of stress σ for RRR Nb–1%Zr at 1200 K and 1300 K (perpendicular to the rolling direction)

In order to describe the stress dependence of the minimum and "plateau" creep rates, respectively, the strain rates $\dot{\epsilon}$ can be plotted as a function of stress in a double–logarithmic manner as shown in the following figures 10 to 12. Plotted are the steady state creep rates and the plateau creep rates (full symbols), respectively, obtained from pure niobium and the alloys containing zirconium as well as the minimum creep rates (open symbols, in the cases of the alloys). The horizontal bars indicate errors in the stress determination caused by uncertainties in measuring the cross sectional areas of the samples. Also plotted in figures 10 to 12 are solid lines which are based on the creep model and which are discussed later in this section. In the case of RRR Nb–1%Zr at 1200 K only the minimum creep rates are plotted. Steady state creep rates could not be obtained at this temperature beacause the plastic strain was not enough, i.e. necking starts early, to establish a steady state region.

As mentioned earlier in this section the shape of the creep curves cannot be attributed to the coarsening of particles, because materials containing particles do not exhibit plateaus over a broad range of strain. Instead, particle strengthened alloys typically exhibit a continuous softening effect. The hypothesis that the investigated alloys do not contain any particles is supported by ongoing TEM investigations which reveal that only a few particles can be found in the zirconium containing alloys. There are far too few particle to explain the difference in strength between the alloys and pure niobium. Therefore coarsening of particles cannot be responsible for the increase in the creep rate after the minimum. A possible explanation for this kind of creep behavior is the coarsening of an inherited fine subgrain structure during (primary) transient creep following the model introduced by Blum and Straub [10, 11]. According to this model the shape of the creep curves can be explained as follows:
The as–received material contains a fine subgrain structure caused by rolling and forging at intermediate temperatures and high stresses during manufacturing. When such a material is tested the shape of the primary transients depends on the applied stress. If the applied stress is large enough to cause a steady state subgrain size w that is equal or smaller than the inherited one, normal transients are observed. In the case when the applied stress causes a steady state subgrain size that is larger than the inherited one, minimum creep rates are observed. The initial decrease in creep rate is due to hardening associated with an increase in the dislocation density in subgrain interiors. After the minimum in the creep rate an increasing creep rate can be seen, because the inherited subgrain size is too small for the applied stress. Therefore the subgrain structure starts to coarsen, which results in an increasing creep rate until a plateau or steady state range of creep is reached.

Based on the model of Blum and Straub an attempt was made to correlate the rate of subgrain coarsening with the creep rate. The following conditions were chosen: RRR Nb–1%Zr, 1300 K, σ = 93.5 MPa. The initial (inherited) subgrain size was $w_0 \approx 1\mu m$. The steady state subgrain size was $w_0 \approx 5\mu m$. [1] According to Blum and Straub the subgrain size as a function

[1] According to personal information of Dr. K. Tanaka, based on TEM investigations

of strain can be calculated as follows:

$$\epsilon = \frac{2n_b}{M}\,\Theta \ln\left(\frac{w}{w_0}\right) \tag{5}$$

where n_b is the number of subgrain boundaries moving in the same direction (= 3, according to Biberger and Blum [4]), M is the Taylor factor (= 2.75) and Θ is the misorientation angle between neighboring subgrains (= 1°). Inserting those quantities into equation 5 one derives the following plot:

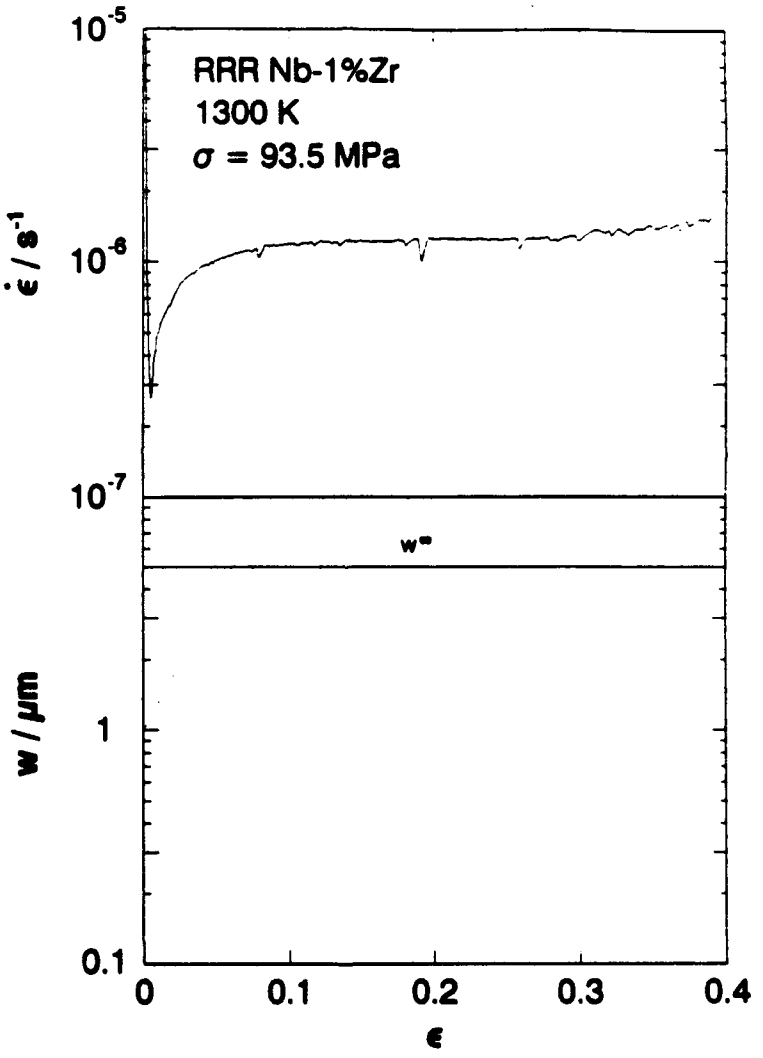

Figure 13: Measured creep rate $\dot{\epsilon}$ and calculated subgrain size w (dotted line) in RRR Nb–1%Zr as a function of strain ϵ

As one can see the model (dotted line starting at $w = 1\mu m$) describes in a fairly good manner the range where coarsening occurs. After approximately 7% strain the subgrain size

has reached the steady state value of $5\mu m$. At this strain the creep rate has also reached the steady state, indicating that the rearranging of the subgrain structure is finished and a steady state subgrain structure is established. The disadvantage Blum and Straub had to deal with during their investigations with the steel X 20 CrMoV 12 was that they had not only to consider the coarsening of subgrains but also the coarsening of carbides. It was difficult for these authors to separate the coarsening processes of the carbides from those of the subgrains. This situation does not hold for the present case. Due to the low content of impurities and the wrapping of the samples prior to testing it is not possible for carbides or particles to form. Therefore this material offered the unique opportunity to investigate the coarsening of subgrains in its simplest form. The Nb–1%Zr alloy can be considered as an opportune model material for the study of the kinetics of subgrain coarsening.

Modelling of the creep rate:

Due to the fact that the minimum creep rates do not play an important role in this material (the minimum creep rate if used in the sense of a particle hardened material is as an artefact in this case), we tried to describe only the plateau or steady state creep rates. We propose that a simple model can be used to describe the creep results. The model is based on an empirical sinh - function:

$$\dot{\epsilon}_{mod} = A\ \sigma^{n_{eff}}\ \sinh\left(\frac{V\,\sigma}{M\,k\,T}\right)\ \exp\left(\frac{-Q}{R\,T}\right) \tag{6}$$

The parameters in the above equation have the following meanings:

A	= Scaling factor
n_{eff}	= effective stress exponent
V	= Activation volume
M	= Taylor factor
k	= Boltzmann's constant
T	= Temperature
Q	= Activation energy
R	= Gas constant

At high stresses the sinh - function takes on an exponentional form, allowing to describe the strain rates at high stresses on the basis of thermally activated glide. At lower stresses equation 6 takes the shape of a power law, allowing to describe the strain rates at those stresses based on climb controlled creep or viscous glide, respectively. For n_{eff} a value of 2 was inserted according to the following equation:

$$n_{eff} = n\ -\ 1 \tag{7}$$

In this equation n is the stress exponent. A value of 3 was inserted, assuming that at very high temperatures and low stresses the natural power law of creep is valid with a stress exponent

of 3, as found by Biberger and Blum [3]. In the case of the alloys at 1300 K a value of 85 b^3 for the activation volume was inserted. This value seems reasonable, if one assumes that the activation volume takes values ranging from 50 to a few hundred b^3. For the activation energy a value of 401 kJ/mole, derived from Frost and Ashby [14], was used. Figures 10 to 12 show that with those parameters the strain rates can be described in a fairly good manner. It can also be seen that the creep behavior of RRR Nb–1%Zr, cut parrallel and perpendicular to the rolling direction, is identical. The modelling did not consider creep rates higher than $1 \cdot 10^{-3} s^{-1}$ in the case of the alloys, because the plastic strain was not enough to establish a steady state creep region. They are therefore plotted in brackets. In the case of RRR niobium an activation volume of 390 b^3 was used to describe the steady state creep rates. As one can see the model describes also the high strain rates in a good manner. This is due to the fact that in this material higher plastic strains are achieved, allowing to establish a steady state creep regime. Due to the lack of enough plastic strain in the case of RRR Nb–1%Zr at 1200 K only the minimum creep rates are plotted. The solid line was calculated assuming constant activation energy. This assumption seems reasonable, because it can be assumed that the activation energy does not dramatically change between 1200 K and 1300 K. The model describes in this case only the upper most three data points. Those values were derived from creep tests with normal primary transients.

4.1.4 The influence of internal oxidizing on the creep behavior of RRR Nb–1%Zr

An important aspect of our original proposal was to internally oxidize and internally nitride the Nb–1%Zr alloy in order to produce a dispersion strenghtened material. In order to do so cp Nb–1%Zr samples were annealed at 1000, 1100, 1200 and 1300 K for 100 hours in vacuum of $1.4 \cdot 10^{-4}$ Pa without wrapping. Samples prepared in this way were tested at 1300 K and stresses of 116 MPa as demonstrated in figure 14. For comparison an as–received sample was tested at the same temperature and stress also without wrapping. The results of these tests demonstrate that the as – received material is the strongest (lowest creep rate) and that annealing without wrapping serves only to soften the material. We presume that the residual oxygen in the retort is sufficient to form zirconia particles in the samples and to overage them at the same time. This assumption is supported by the fact that the higher the temperature the softer the material became because the kinetics (diffusion processes) are faster at higher temperatures.

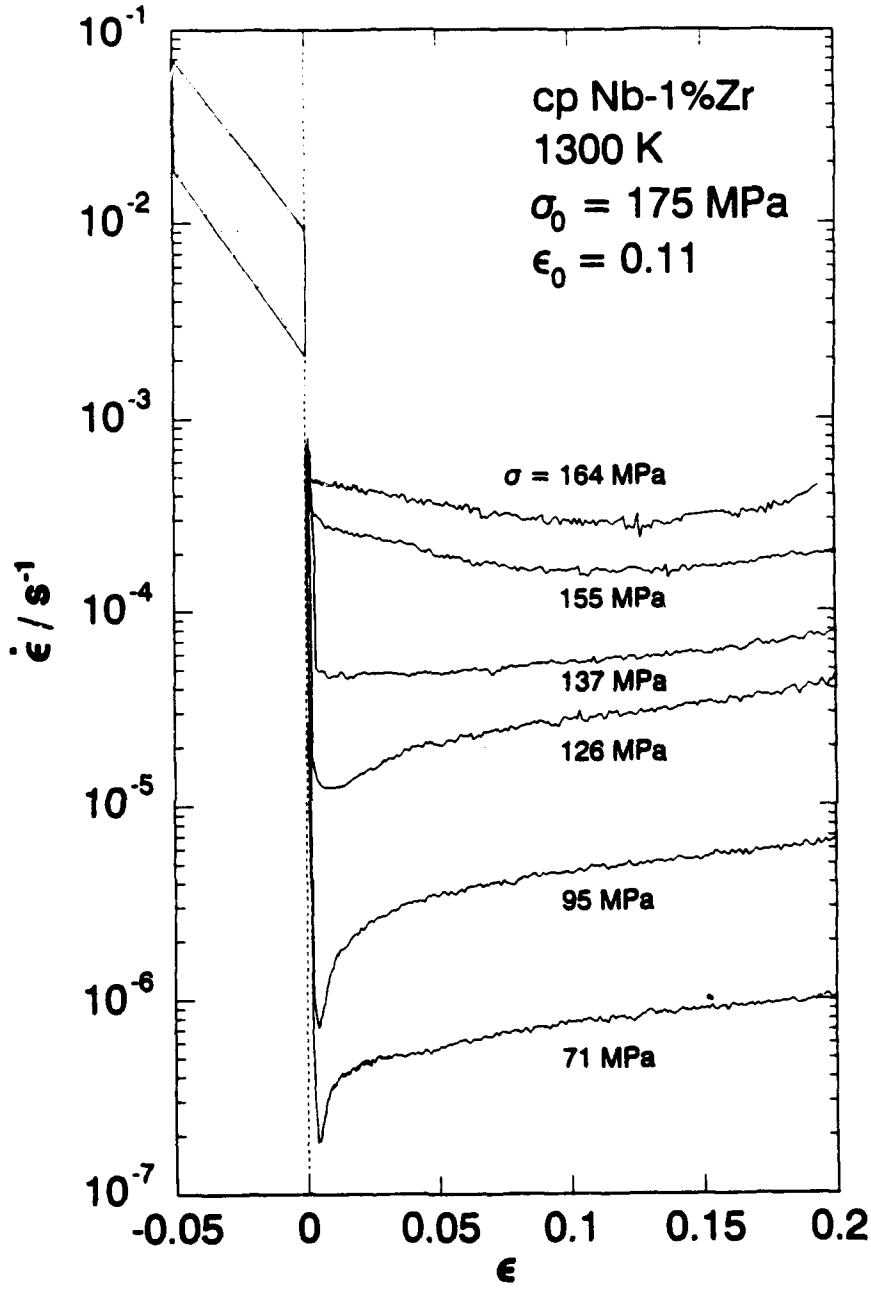

Figure 14: Creep rate $\dot{\epsilon}$ as a function of strain ϵ for cp Nb–1%Zr as – received and annealed in vacuum and tested at 1300 K at 116 MPa

4.2 Stress reduction tests

Stress reduction tests were performed in order to determine the rate controlling mechanism in creep. During steady state deformation the processes of work hardening and recovery are coupled. To investigate those mechanisms individually it is necessary to decouple them. This can be achieved by performing stress reduction tests as demonstrated by Blum, Rosen, Cegielska and Martin [8]. In the present work stress reduction tests were performed on cp Nb–1%Zr and RRR Nb–1%Zr at 1300 K.

4.2.1 Creep rate as a function of strain

Figure 15 shows the creep rate $\dot{\epsilon}$ as a function of the strain ϵ for cp Nb–1%Zr. The creep curves are plotted in a manner so that the stress reduction starts at strain 0. The samples were deformed at an initial stress $\sigma_0 = 175$ MPa until a steady state range of creep was reached at approximately $\epsilon = 0.11$. The stress was then reduced by various amounts (see figure 15) and the creep reponse was monitored.

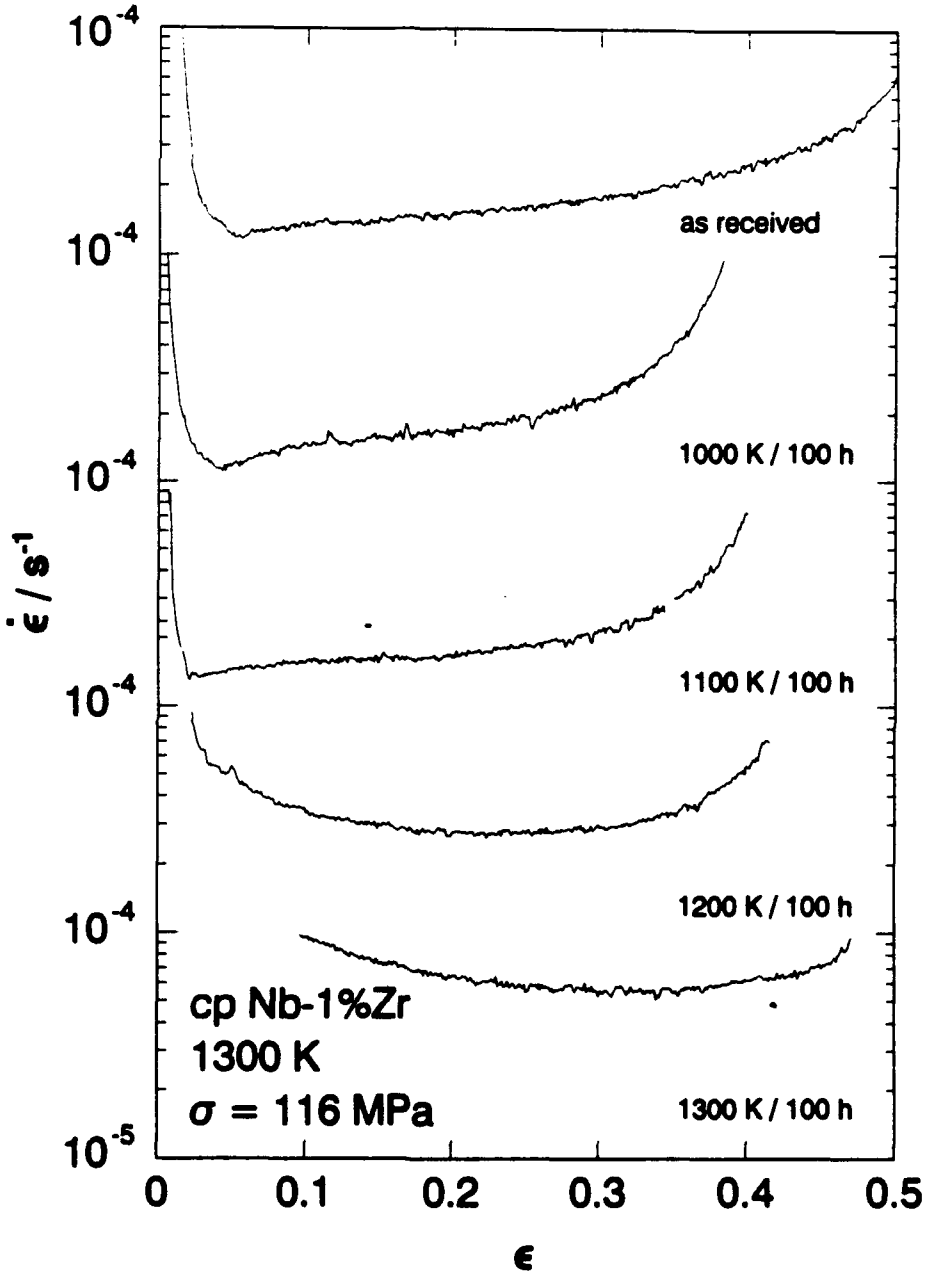

Figure 15: Creep rate $\dot{\epsilon}$ as a function of strain ϵ for cp Nb–1%Zr tested at 1300 K at an initial stress σ_0 of 175 MPa

The secondary transients shown in figure 15 are very similar to the creep responses for pure materials (see Müller, Biberger and Blum [15]). After a small reduction in stress the creep rate increases after an initial drop to reach the new steady state. After a large stress reduction the transients are quite different. After the initial drop the creep rate decreases until a minimum is reached. The minimum is followed by an increasing creep rate until the new steady state regime is reached again. According to Blum et al. it is assumed that after small reductions in stress the work hardening term is dominating whereas, after large reductions in stress the recovery term is dominating. In order to prove this matter for the present material the so–called reduced creep rate $\dot{\epsilon}_r$ can be plotted as a function of stress σ. The reduced creep rate is the creep rate measured "immediately" after the elastic reaction of the sample. For details in evaluating $\dot{\epsilon}_r$ see Blum, Vogler, Biberger and Mukherjee [9].

4.2.2 Creep rate at constant dislocation structure as a function of stress

Figure 16 is a semilogarithmic plot of the reduced creep rate $\dot{\epsilon}_r$ normalized by the initial creep $\dot{\epsilon}_0$ as a function of the reduced stress σ normalized by the initial stress σ_0. The tests were performed on RRR Nb–1%Zr at 1300 K. A comparison was made between cp and RRR Nb–1%Zr with respect to the creep behavior after stress reduction. No qualitative difference between the two materials could be found.

The stress reduction tests were performed when a steady state range of creep was reached, usually between strains of 0.17 and 0.24. The initial stress σ_0 was 190 MPa, which resulted in initial (steady state) creep rates $\dot{\epsilon}_0$ typically in the range of $4 \cdot 10^{-4}s^{-1}$ and $6 \cdot 10^{-4}s^{-1}$. Figure 16 shows that the high stress branch of the $\dot{\epsilon}_r(\sigma)$ – curves is straight with a relatively steep slope. With decreasing σ/σ_0 the slope decreases. The value of σ/σ_0 where the slope changes is about the same as that value of σ/σ_0 where the shape of the $\dot{\epsilon}_r$-ϵ – curve changes from monotonic to nonmonotonic (at stresses of approximately 137 MPa, see figure 15). As pointed by out by Blum et al. [8], this change in transient creep behavior suggests that it is necessary to distinguish between two different mechanisms of dislocation motion during creep. Mechanism 1 with large stress sensitivity and $d\dot{\epsilon}/d\epsilon \geq 0$ dominates at relatively large stresses, while mechanism 2 with small stress sensitivity and $d\dot{\epsilon}/d\epsilon \leq 0$ becomes apparent for small relative stresses. We shall designate the corresponding contributions to the creep rate $\dot{\epsilon}_r$ as $\dot{\epsilon}_{r1}$ and $\dot{\epsilon}_{r2}$, respectively:

$$\dot{\epsilon}_r = \dot{\epsilon}_{r1} + \dot{\epsilon}_{r2} \tag{8}$$

As shown in figure 16, $\dot{\epsilon}_{r1}$ can be represented by a straight line on a semi – logarithmic plot. This means that $\dot{\epsilon}_{r1}$ depends exponentially on stress.

The other component, $\dot{\epsilon}_{r2}$, can be drawn without constraint in such a manner that it extrapolates to $\dot{\epsilon}_{r2}/\dot{\epsilon}_0 = 0.1$ at $\sigma/\sigma_0 = 1$. It should be noted that even at $\sigma/\sigma_0 \approx 0$, i.e. after nearly full unloading, a positive creep rate $\dot{\epsilon}_{r2}$ is measured after the anelastic back flow. This observation indicates that there are not only long range internal back stresses existing in

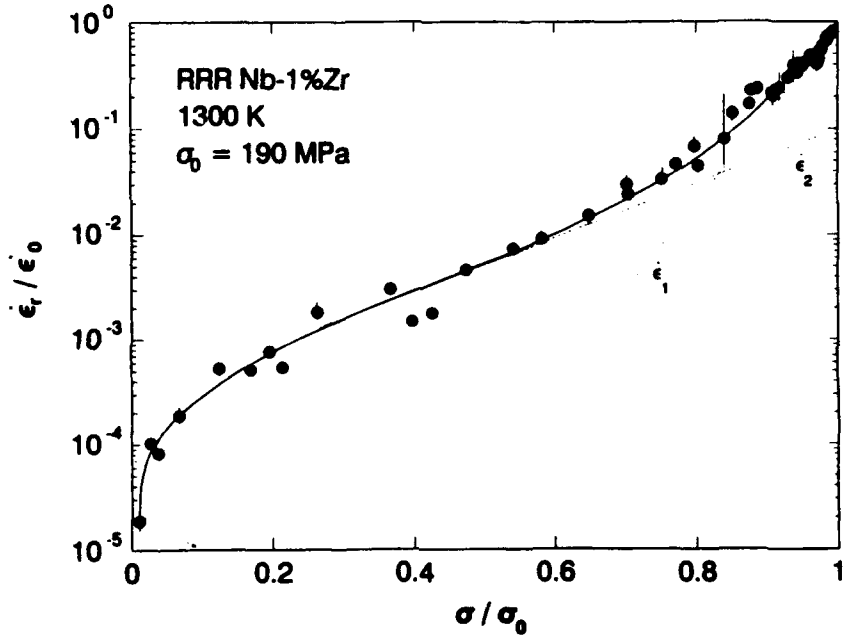

Figure 16: Reduced creep rate $\dot{\epsilon}_r$ normalized by the initial creep rate $\dot{\epsilon}_0$ as a function of the reduced stress σ normalized by the initial stress σ_0 for RRR Nb–1%Zr at 1300 K

the deformed material causing anelastic back flow after unloading, but also internal forward stresses causing forward flow when anelastic back flow has ceased.

According to Blum et al. [9] the term $\dot{\epsilon}_{r2}$ can be interpreted as the strain rate associated with recovery of the dislocation structure. This interpretation is based on the concept that the balance between generation and annihilation of dislocations is disturbed after a stress reduction, such that glide associated with generation of dislocations is suppressed, while recovery of the dislocation structure goes on and the dislocation structure coarsens until the new steady state is reached. Following Müller, Biberger and Blum [15] the term $\dot{\epsilon}_{r2}$ can be attributed to the migration of subgrain boundaries. As shown above this also holds for Nb–1%Zr: the term $\dot{\epsilon}_{r2}$ can easily be extrapolated to 0.1 for $\sigma/\sigma_0 \rightarrow 1$. This means that also in Nb–1%Zr the recovery migration of subgrain boundaries is the rate controlling mechanism. As pointed out earlier the term $\dot{\epsilon}_{r1}$ shows an exponential stress dependence. According to Blum et al. [8] and Nakayama and Gibeling [17] this term can be associated with work hardening. The authors suggested that for a great number of pure materials, thermally activated glide due to cutting of forest dislocations is the work hardening mechanism. In order to check this for Nb–1%Zr we calculated an apparent activation Δa from our results according to the

following equation:

$$\Delta a = \frac{MkT}{b} \frac{\partial \ln \dot{\epsilon}}{\partial \sigma} \tag{9}$$

following Nadgorny [16] a true activation area $\Delta a'$ can be calculated $\Delta a' = 1.5\Delta a$. This true activation area can now be compared with the dislocation spacing in the subgrain interior. Blum et al. [8] demonstrated, that there is a good agreement with the dislocation spacing and the true activation area. A comparison for Nb–1%Zr is shown in the following figure: According to equation 4 the dislocation spacing in the subgrain interior is proportional to

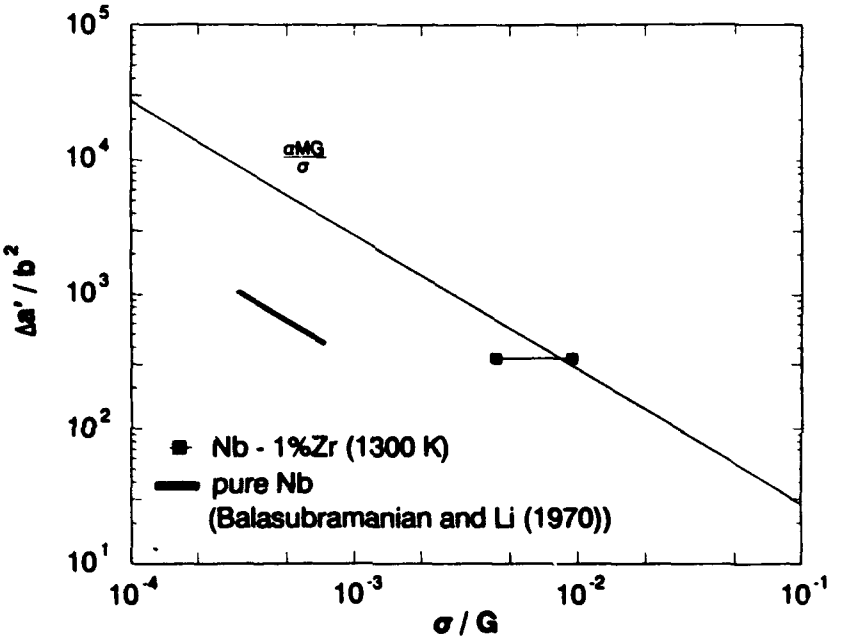

Figure 17: True activation area $\Delta a'$ normalized by b^2 as a function of σ/G

G/σ. As figure 17 shows there is not a good agreement between the dislocation spacing in the subgrain interior and the true activation area. The large horizontal error bar is due to the uncertainty in determining the shear modulus. As an upper limit for G we have chosen the value for pure niobium derived from Frost and Ashby [14]. As the lower limit the shear modulus was calculated from the Young's modulus obtained from our own measurements. We assume that the reason for the disagreement in activation areas can be found in the strong solid solution hardening effect active in Nb–1%Zr at lower temperatures. The true activation area is therefore shifted towards lower values. Also plotted in this figure are values for the activation area derived from Balasubramanian and Li [2] for pure niobium at temperatures between 1223 K and 1273 K. The data from those authors are also below the line representing the dislocation spacing. The reason for this deviation is not clear at present. A plausible explanation could be that at even lower temperatures one observes a change in the dominating creep mechanism, probably from thermally activated dislocation intersection to Peierls mechanism. Another

explanation could be the different technique the authors used to determine the activation area. Namely by increasing the stress and measuring the creep response. We believe that the latter case is the more likely one.

4.3 References for creep

References

[1] Arndt, R., *Zeitschrift zur Metallkunde* **60** (1969) 29

[2] Balasubramanian, N. and Li, J. C. M., *Journal of Materials Science* **5** (1970) 434

[3] Biberger, M. and Blum, W., *Scripta Metall.* **23** (1989) 1419

[4] Biberger, M. and Blum, W., Part II, *Phil. Mag.*, march 1992

[5] Biberger, M., Davidson, M. and Mukherjee, A.K., submitted to *Acta metall.*

[6] Blum, W., Absenger, A. and Feilhauer, R., *Proc. 5th Int. Conf. on the Strength of Metals and Alloys*, Aachen (1979) p. 265

[7] Blum, W. and Reppich, B., "Creep Behaviour of Crystalline Solids", Vol. 3 in the Series Progress in Creep and Fracture, Pineridge Press, Swansea, U.K., (1985) S. 83

[8] Blum, W., Rosen, A., Cegielska, A. and Martin, J.L., *Acta metall.* **37** (1989) 2439

[9] Blum, W., Vogler, S., Biberger, M. and Mukherjee, A.K., *Mater. Sci. Eng.* **A 112** (1989) 93

[10] Blum, W. and Straub, S., *Steel Research* **62** (1991) No.2 72

[11] Blum, W. and Straub, S., "Evolution of creep rate and microstructure during creep of X 20 CrMoV 12 1", in: 8th International Symposium on Creep – Resistant Metallic Material, Sept. 17–19, Zlín, Czechoslovakia

[12] Brinson, G. and Argent, B.B., *J. Inst. Met.* **91** (1962) 293

[13] Davidson, M., Biberger, M. and Mukherjee, A.K., submitted to *Acta metall.*

[14] Frost, H.J. and Ashby, M.F., Deformation Mechanism Maps, Pergamon Press, (1982)

[15] Müller, W., Biberger, M. and Blum, W., Subgrain Boundary in LiF during Creep. Part III, *Phil. Mag.* april 1992

[16] Nadgorny, E., Dislocation Dynamics and Mechanical Properties of Crystals, *Progress in Materials Science* (1988) Vol. 31 (Oxford: Pergamon Press)

[17] Nakayama, G. S. and Gibeling, J.C., *Acta metall.* **38** (1990) 2023

[18] Vandervoort, R.R., *Trans AIME* (1969) **245** 2269

5 LOW CYCLE FATIGUE RESULTS AND DISCUSSION

Several investigations have been made of the mechanisms of cyclic deformation of single crystals of niobium [1,2,3]. However, very little is known regarding the fatigue behavior of polycrystalline niobium [4]. Chung and Stoloff [5] tested pure polycrystalline niobium under total strain control at a constant frequency. To investigate the fatigue mechanisms, however, it is necessary to use plastic strain as the controlled variable [6].

Basic research on cyclic deformation of FCC crystals, primarily copper, has resulted in fairly complete understanding of the fatigue mechanisms. In contrast, relatively little fundamental research has been reported for BCC metals and a detailed, mechanistic understanding is still lacking. However, it has been shown that the cyclic deformation of BCC metals is sensitive to temperature, strain rate, and direction of deformation [1,2,6].

At low temperatures ($T < 0.2\ T_m$) or high strain rates at $T \approx 0.2\ T_m$, BCC metals exhibit a deformation response that is strongly dependent on temperature or strain rate, $\dot{\epsilon}$. The dependence of the flow stress on temperature and strain rate is usually expressed in terms of an athermal stress and an effective stress as follows [1,6]:

$$\sigma = \sigma_G + \sigma^*(\dot{\epsilon}, T) \tag{10}$$

where σ_G is the athermal component that arises from the long range interaction of gliding dislocations with the structure and varies weakly with temperature to the same degree as the shear modulus, and σ^* is the effective stress that depends on $\dot{\epsilon}$ and T but only weakly on the density and arrangement of the dislocations.

In commercially pure niobium, as with other BCC metals, the physical source of the large effective stress is the limited mobility of the screw dislocations at low temperatures. The glide of the screw dislocations occurs by thermally activated formation of kink pairs. As a result, the mobility of the screw dislocations decreases strongly when the temperature decreases below a critical temperature. For niobium, this critical temperature is close to room temperature for slow strain rates, but is higher than room temperature for fast strain rates [1]. In the low temperature regime, the edge dislocations are more mobile than the screw dislocations, and dislocation multiplication by bowing is difficult. Above the critical temperature, both screw and non – screw segments have similar mobilities, σ^* is small and the deformation behavior resembles that of FCC metals.

Besides this stress dependence, the cyclic response of BCC metals is different from that of FCC metals. In single crystals, a slip plane and stress asymmetry in tension and compression is observed [6,7]. In cyclic testing, this asymmetry leads to shape changes in the crystals. The slip plane and stress asymmetry is attributed to the extended core structure of the screw dislocations in BCC metals. The effect of the extended core structure is to cause the screw

dislocation motion to be dependent not only on the shear stresses in the slip plane but also on the non-shear components, hence the tension/compression asymmetry [8].

The few available studies of BCC single crystals provide useful information regarding the mechanisms of cyclic deformation. However, no corresponding fundamental studies of polycrystalline metals have been reported. Therefore, the purpose of this investigation was to study the low cycle fatigue mechanisms in polycrystalline niobium. For comparison, the solid solution hardened niobium 1%zirconium (Nb–1%Zr) alloy was tested in addition to the commercially pure niobium (cp Nb). In particular, our goal was to identify the effects of strain rate (or temperature) on the cyclic response and to compare the polycrystalline data to the single crystal results available in the literature.

In order to fully characterize the cyclic deformation behavior of niobium, it was necessary to conduct tests under two separate conditions 1) where the effective stress was negligible and 2) where the effective stress was a significant fraction of the total stress. Rather than changing the temperature from ambient, the plastic strain rate was varied. The fast ($2 \cdot 10^{-2}s^{-1}$) and slow ($2 \cdot 10^{-4}s^{-1}$) plastic strain rates were chosen, based on the single crystal data of Ackermann, et al. [1], such that the effective stress would be significant at the fast strain rate but negligible at the slow strain rate. In this way it was possible to examine the complete range of dislocation behavior in the cyclic deformation of niobium.

5.1 Monotonic stress-strain curves

The data acquired during the first quarter cycle of the highest plastic strain amplitude fatigue tests were used as the monotonic stress-strain curves. These results are shown in figure 18. For both materials, higher stresses were recorded at the fast strain rate compared to the slow strain rate, as expected. There is a smaller difference in stress between the monotonic stress-strain curves for the Nb–1%Zr tested at the two rates due to the fact that solute atoms limit edge dislocation mobility, thereby shifting the low temperature friction stress controlled regime to higher strain rates (lower temperatures). The absence of a yield point in the cp Nb is consistent with the relatively low interstitial content of this material. The curves for Nb–1%Zr show an upper yield which we attribute to the pinning of dislocations by the substitutional zirconium atoms.

5.2 Elastic moduli

In order to calculate the plastic strain, the elastic strain must be subtracted from the total strain. This calculation requires that the elastic modulus be known to a high degree of accuracy. In the present work the elastic moduli were obtained by deforming specimens well within the elastic limits. The measured moduli were 91.8 and 105.1 GPa for the cp Nb and

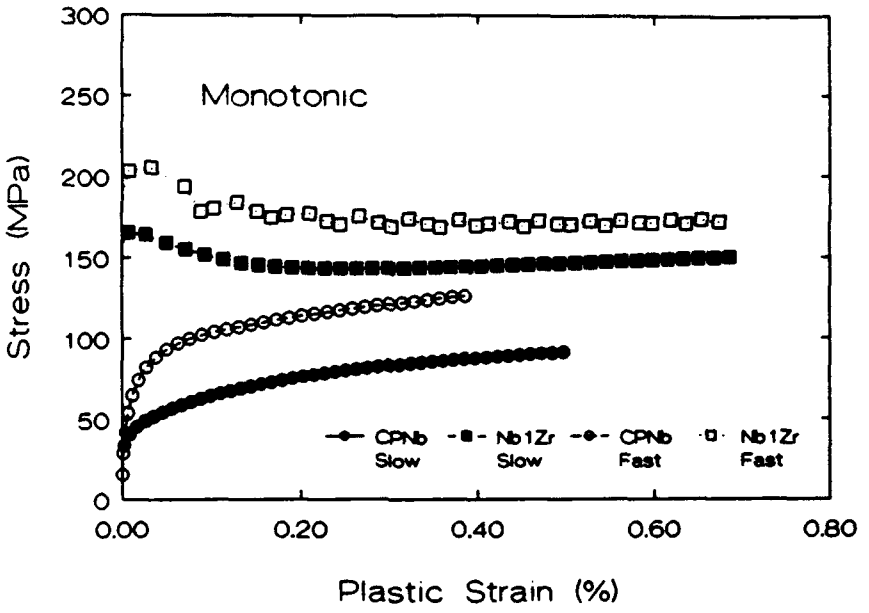

Figure 18: Monotonic stress-strain curves for commercially pure Nb and Nb–1%Zr each at two strain rates

Nb–1%Zr metals, respectively. Published modulus values are 105 GPa and 68.9 GPa for cp Nb and Nb–1%Zr, respectively [9].

The difference between the published and measured values for cp Nb is probably a result of crystallographic texture in the material used in the present investigation, since the material was not completely recrystallized prior to testing. The reason for the discrepancy in the modulus values for Nb–1%Zr is not clear. However, it is difficult to accept that the addition of one percent zirconium to niobium would decrease the elastic modulus by one-third; for this reason we believe the published value of 68.9 GPa to be erroneous. The measured value of 105 GPa for Nb–1%Zr is certainly more consistent with the accepted modulus value for cp Nb.

5.3 Cyclic stress-strain response

For each metal and strain rate, a series of tests was conducted over a range of plastic strain amplitudes. There were no significant differences between the magnitudes of the tension and compression peak stresses, in contrast to single crystal results, but as expected for polycrystalline material. Figures 19 through 22 illustrate the average (of the tension and compression) peak stress versus number of cycles for the two metals tested at the two strain rates.

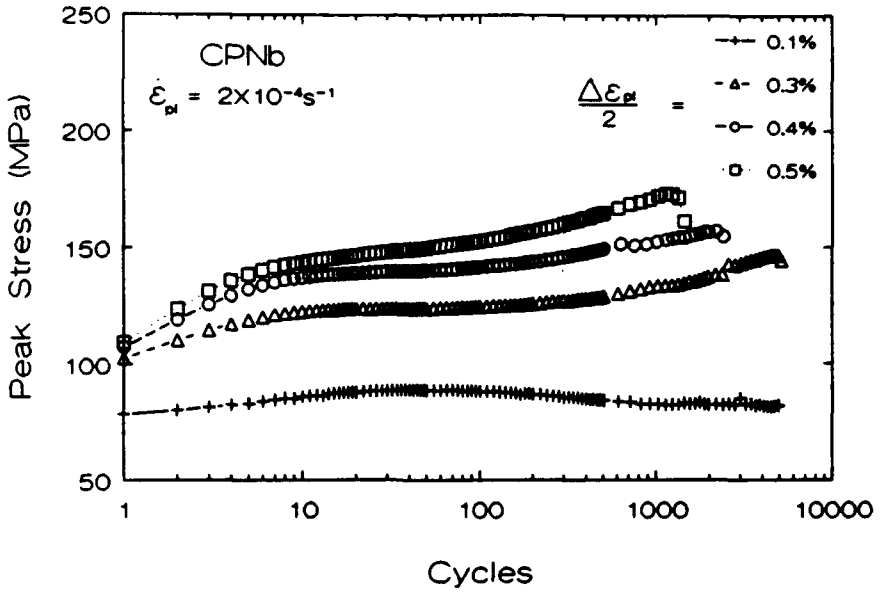

Figure 19: Peak stress versus number of cycles for commercially pure Nb tested at the slow strain rate

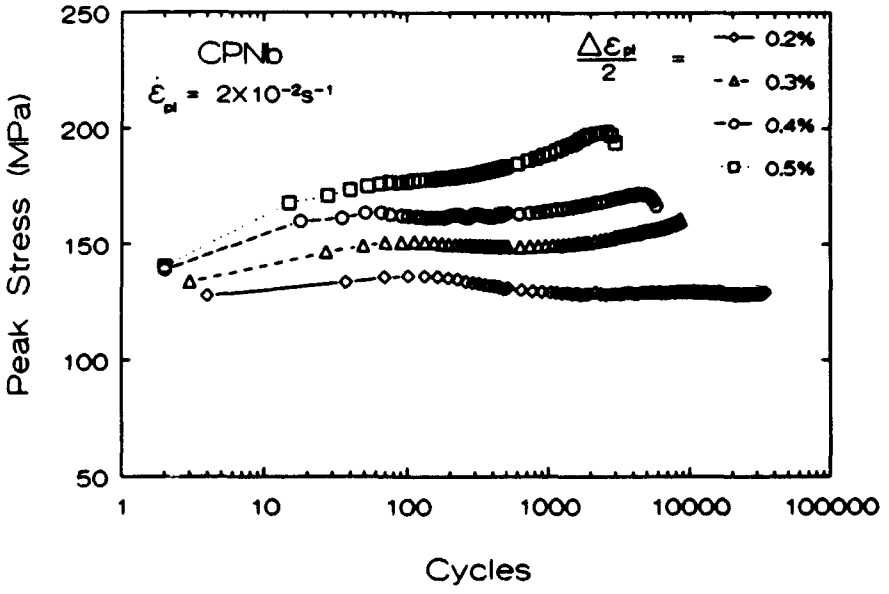

Figure 20: Peak stress versus number of cycles for commercially pure Nb tested at the fast strain rate

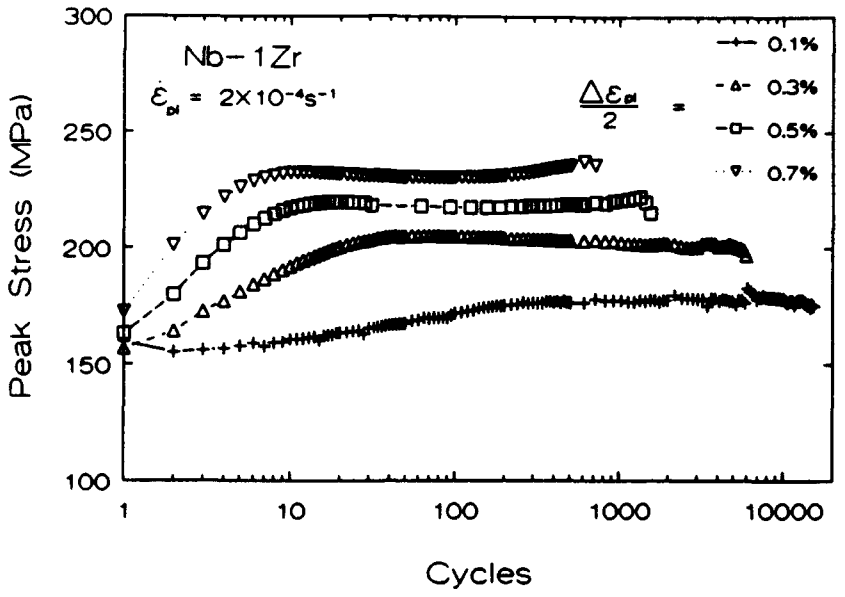

Figure 21: Peak stress versus number of cycles for Nb–1%Zr tested at the slow strain rate

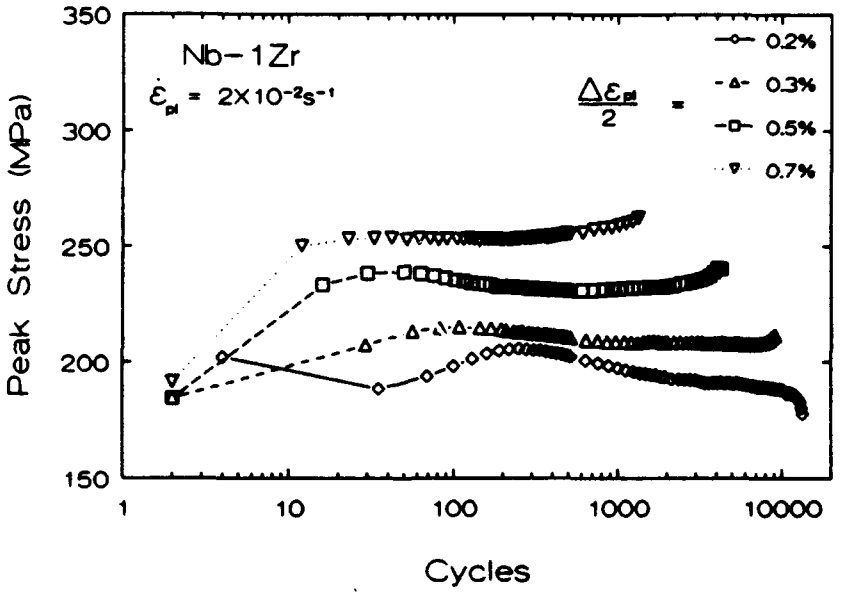

Figure 22: Peak stress versus number of cycles for Nb–1%Zr tested at the fast strain rate

For most specimens, an initial period of rapid hardening was observed, after which the peak stress remained relatively stable. In particular, the results for Nb–1%Zr show stable behavior after the initial rapid hardening regime, although a small amount of softening occurred at the high rate (figure 22). In contrast, the results for cp Nb exhibit either stable behavior or a gradual increase in peak stress with increasing number of cycles at the higher plastic strain amplitudes (figures 19 and 20). In the latter case, the rate of increase in stress is proportional to the plastic strain amplitude.

Cyclic stress-strain (CSS) curves can also be constructed from the present data. The peak stress and plastic strain values from a stable hysteresis loop are obtained from each test. Plotting and linking these stress-strain data points produces the CSS curve. Most of the tests in this investigation resulted in stable hysteresis loops. For those that did not, the stress and strain values at the middle of the life were used in the construction of the CSS curves. In all cases the average (of the tension and compression) peak stress was used.

In most cases, an individual specimen was used to obtain each of the cyclic stress-strain data points. An alternative approach for obtaining the CSS is the multiple step test in which a single specimen is first cycled between set plastic strain limits until a stable hysteresis loop is formed. The plastic strain limit is then increased and the specimen again cycled until another stable hysteresis loop is formed. It has been shown that such tests yield essentially equivalent responses to those of constant amplitude tests provided the material deforms by wavy slip [10]. The cp Nb data points for $\Delta\epsilon_{pl}/2$ from 0.02 to 0.1 % at the fast strain rate were obtained from a multiple step test. The validity of the multiple step data was confirmed, since excellent correlation was obtained with multiple step and individual specimen data points at plastic strain amplitudes of 0.2, 0.3, and 0.4 percent.

The CSS curves of the two metals, each tested at two strain rates, are shown in figure 23. Only cyclic hardening was observed, which is typical for annealed metals. The differences in stress for the two rates arises because lattice friction (Peierls stress) limits the mobility of screw dislocations at fast rates (low temperature). As in the case of the monotonic stress-strain curves, there is a smaller difference in stress for the Nb–1%Zr tested at the two rates due to the fact that the edge dislocation mobility is limited by the solute atoms.

Another consequence of the limited screw dislocation mobility in BCC metals at fast strain rates is the occurrence of a plateau in the cyclic stress-strain curves at low plastic strain amplitudes. The plateau consists of a range of small plastic strain amplitudes over which the cyclic stress does not vary. Such plateaus have been found in the cyclic stress-strain curves of single crystals of α – iron and α – iron polycrystals [6,11,12] and niobium single crystals [13,14]. It is interesting that for the α – iron polycrystals the plateau was present under constant plastic strain rate testing, but not at constant frequency. With α – iron single crystals, this kind of plateau was not observed at slow strain rates [12]. This microplastic plateau is caused by a very low hardening rate due to the restricted mobility of the screw dislocations [6]. The restricted mobility makes dislocation multiplication by irreversible bowing a difficult process.

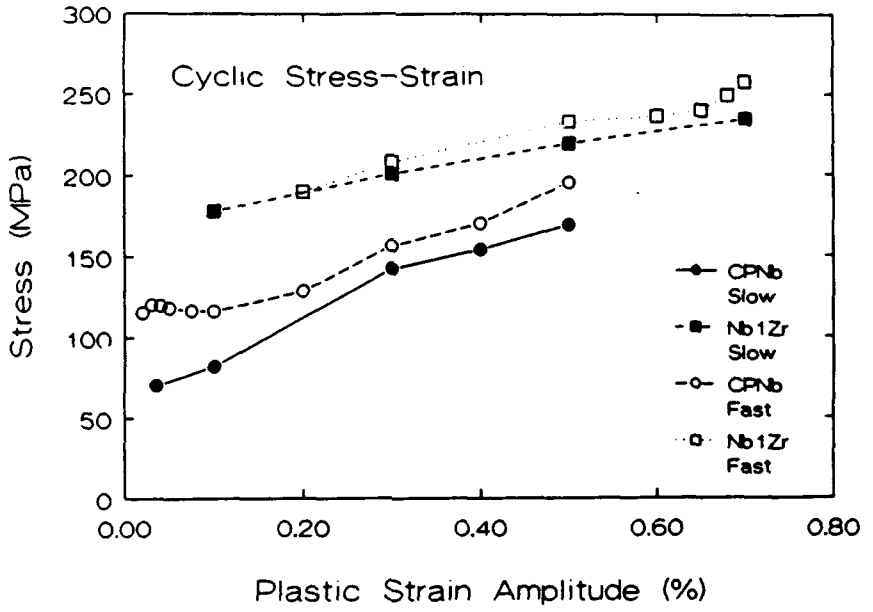

Figure 23: Cyclic stress-strain curves for commercially pure Nb and Nb–1%Zr

As a consequence, deformation in this regime occurs by the reversible to-and-fro motion of edge dislocations [13].

As shown in figure 23, the cp Nb material tested at the fast strain rate exhibited a microplastic plateau at plastic strain amplitudes equal to and below 0.1%. At the slow strain rate there was no microplastic plateau. In fact, a microplastic plateau is not expected at the slow strain rate because the mobilities of the edge and screw dislocations are comparable and therefore dislocation multiplication should not be restricted. In a similar manner, the Zr atoms lower the mobility of edge dislocations in the Nb–1%Zr alloy to a level comparable to that of screw segments, and a microplastic plateau is not expected at either strain rate. For this reason, as well as the operational difficulty of testing this material at plastic strain amplitudes in the region of the upper yield point, the low strain behavior of Nb–1%Zr was not explored in this work.

The data of Mughrabi and coworkers [13,14], exhibit a microplastic plateau in niobium single crystals at plastic strain amplitudes less than 0.05% with a plateau stress of 20 MPa. Mughrabi used a Schmid factor of 0.5; hence the plateau shear stress was 10 Mpa. Assuming a Taylor factor of 3, the equivalent polycrystalline tensile stress is 30 MPa. The results of this investigation presented in Figure 7 show a microplastic plateau at plastic strain amplitudes less than 0.1% with a plateau tensile stress of 115 MPa. The large difference in plateau stress is attributed to the very high purity of the crystals used by Mughrabi and to the fact that single crystals are generally much softer.

The existence of the microplastic plateau has been proposed as the physical basis for the fatigue limit in iron [13]. In conventional fatigue tests the strain rate is high, indicating that the mobility of screw dislocations should be restricted. When the plastic strain range is small, the plastic strain can be accommodated by the reversible motion of the edge dislocations without microstructural changes and without noticeable cyclic hardening. Therefore, at high strain rates, Mughrabi [6] has suggested that the fatigue limit of BCC metals should " . . . correspond rather well to the plateau of the cyclic stress-strain curve and should lie slightly below the macroscopic yield stress of the virgin material measured at the strain-rate of the fatigue tests." The 0.2% offset yield strength measured at the fast strain rate was 124 MPa, which is only slightly higher than the microplastic plateau stress of 110 MPa, in agreement with this prediction. A fatigue limit for polycrystalline niobium [9] is listed as 138 MPa which is roughly comparable to the 110 MPa plateau stress measured in the present study. Thus, the results of this investigation support the concept that the limited mobility of screw dislocations in the microplastic plateau is the physical basis for the fatigue limit.

The absence of a microplastic plateau at the slow strain rate suggests the lack of a fatigue limit. This observation has important engineering implications since our practical understanding of fatigue in BCC metals (including steel) is based on the concept of a fatigue limit. However, most fatigue tests are conducted at high rates to minimize testing time, whereas service conditions may impose lower loading rates where the intrinsic material behavior is different. It may be necessary to reconsider the concept of the fatigue limit in light of the fundamental effects of strain rate and solute content on dislocation mobility.

5.4 Intergranular crack initiation

As noted earlier, the low temperature (high strain rate) deformation of BCC metals is dominated by the mechanisms of screw dislocation glide. One important aspect of this behavior is the slip plane and stress asymmetry between tension and compression loading of single crystals. In polycrystalline BCC metals, however, a macroscopic tension/compression asymmetry is not expected. Instead, the effect of the individual grain shape changes due to local tension/ compression asymmetry under cyclic loading at high strain rates is to make intergranular cracking more probable. In experiments on iron-based alloys, Magnin and Driver [15] found that fatigue crack initiation was intergranular at high strain rates and transgranular at low strain rates. This observation is consistent with the expected glide behavior of screw dislocations at the two rates. Even without the tension/compression asymmetry in individual crystals some incompatible deformation occurs, but the tension/compression asymmetry accentuates the incompatible deformation thus increasing the probability of intergranular cracking. The cp Nb and Nb–1%Zr specimens tested at the fast strain rate exhibited intergranular secondary cracking as shown in figure 24. In contrast, there were no cracks that could be clearly identified as intergranular cracks in the cp Nb or Nb–1%Zr specimens tested

at the slow strain rate.

Figure 24: Intergranular cracking observed in a commercially pure Nb specimen tested at the fast strain rate

5.5 Cyclic life

Figure 25 illustrates the fatigue-life data (Coffin-Manson plot) of plastic strain amplitude versus number of reversals to failure. As mentioned previously, both 90 degree and 180 degree extensometer knife edges were used in the present experiments. The data form two nearly parallel lines. In the lower line, all of the specimens, except one, were tested with the 90 degree knife edges. In the upper line, all specimens were tested with 180 degree knife edges. The upper and lower lines drawn in figure 25 are linear fits to the logarithmic data for the 180 degree (blunt) and 90 degree (sharp) knife edges, respectively. The deeper impressing 90 degree knife edges caused shorter life relative to the 180 degree knife edges; this was confirmed in duplicate tests of Nb–1%Zr at a plastic strain amplitude of 0.4%. Thus, the offset between the two lines formed by the data can be attributed entirely to the use of different knife edges.

We conclude that there is no significant difference in cyclic life between the two metals and there is no influence of strain rate on cyclic lifetime.

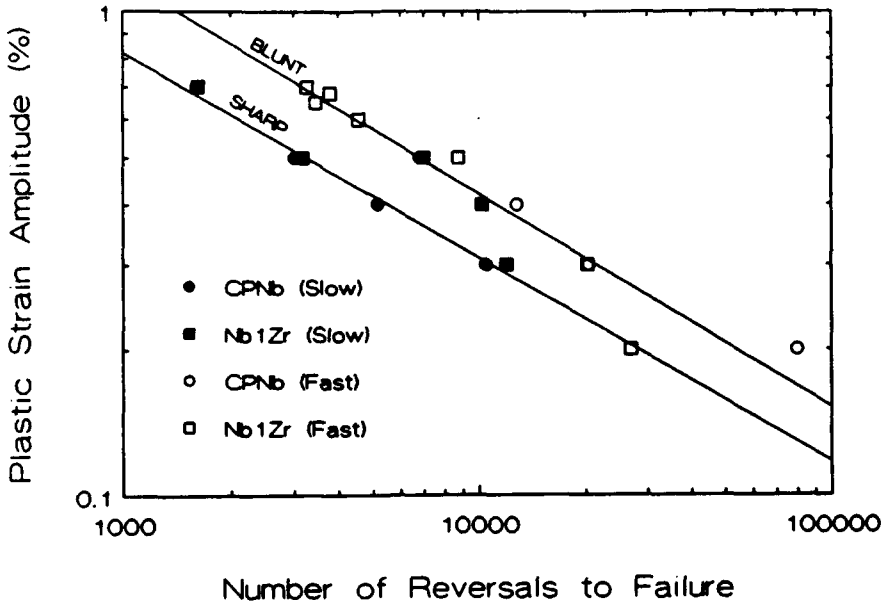

Figure 25: Coffin-Manson plot for commercially pure Nb and Nb–1%Zr

5.6 Hysteresis loop analysis

During the course of this investigation, it was noted that although the peak stress did not vary significantly with increasing numbers of cycles, the shape of the hysteresis loops did change. As a consequence, a detailed analysis of the hysteresis loops produced during low cycle fatigue testing was conducted in order to determine the friction stress and back stress components for each loop, following a procedure outlined by Kuhlmann-Wilsdorf and Laird [16]. For each loop, a peak stress, σ_p and a yield stress, σ_y can be identified with both right and left sides of the loop, as shown in figure 26. The friction stress, σ_f and back stress, σ_b are simply determined as follows:

$$\sigma_p = \sigma_f + \sigma_b \tag{11}$$

$$\sigma_y = \sigma_f - \sigma_b \tag{12}$$

Rearranging,

$$\sigma_f = \left(\frac{\sigma_p + \sigma_y}{2}\right) \tag{13}$$

$$\sigma_b = \left(\frac{\sigma_p - \sigma_y}{2}\right) \tag{14}$$

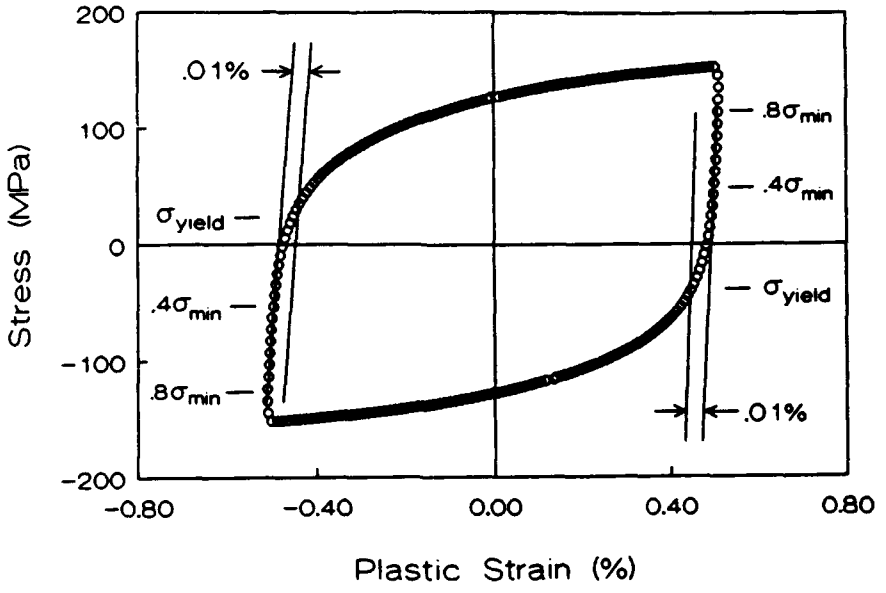

Figure 26: Hysteresis loop showing definition of yield stress

The value of the yield stress, however, is somewhat arbitrarily determined, just as the monotonic yield strength is dependent on the arbitrary choice of an offset (typically 0.2%) as the defining value. In the present analysis, the data points between 0.4 and 0.8 times the peak stress were used to define a straight line (determined from a least squares fit), since this was the most linear section of that part of the loop. Another straight line parallel to the first, but offset from it by 0.01% strain, was constructed. The yield stress was defined as the intersection of this second line with the hysteresis loop. A constant offset parameter of 0.01% strain was used for all tests, therefore at least the relative values of the friction and back stresses are meaningful.

The peak stresses of the Nb–1%Zr samples at both slow and fast strain rates were constant after the short rapid hardening of the first few cycles. Constant peak stresses are often considered to indicate a stable mechanical and microstructural condition. However, the hysteresis loop analysis demonstrates that the constant peak stresses for Nb–1%Zr were a result of the increasing back stress compensating for the decreasing friction stress component. An example of this result is shown in figure 27. Thus, a constant peak stress does not necessarily mean a stable condition during cyclic deformation.

The following comments pertain to the behavior after the initial rapid hardening phase of the first few cycles. As shown in figure 20 and 21, the plots of peak stress versus number of cycle for the cp Nb samples tested at plastic strain amplitudes of 0.3, 0.4 and 0.5% showed slight but gradually increasing peak stress with increasing numbers of cycles. The results of the

hysteresis loop analysis demonstrate that the increasing peak stress was due to an increasing back stress; the friction stress remained essentially constant as indicated in the example shown in figure 28. A comparison of figures 27 and 28 shows a similarity of increasing back stress with increasing numbers of cycles for both metals. In contrast, the friction stress remained constant during cycling of cp Nb and gradually decreased in Nb–1%Zr.

The two metals also exhibited a different effect of strain rate on the friction stress. It can be seen in figure 29 that the results for cp Nb always exhibit a greater friction stress at the fast strain rate compared to the slow strain rate. This was not true for Nb–1%Zr, where three out of four samples exhibited a lower friction stress at the fast strain rate. In cp Nb, the friction stress has a strong Peierls stress component which accounts for it's strain rate sensitivity. In Nb–1%Zr, the friction stress is dominated by the zirconium atoms and the Peierls stress component is negligible at room temperature, with the consequence that the strain rate sensitivity of the friction stress is greatly reduced.

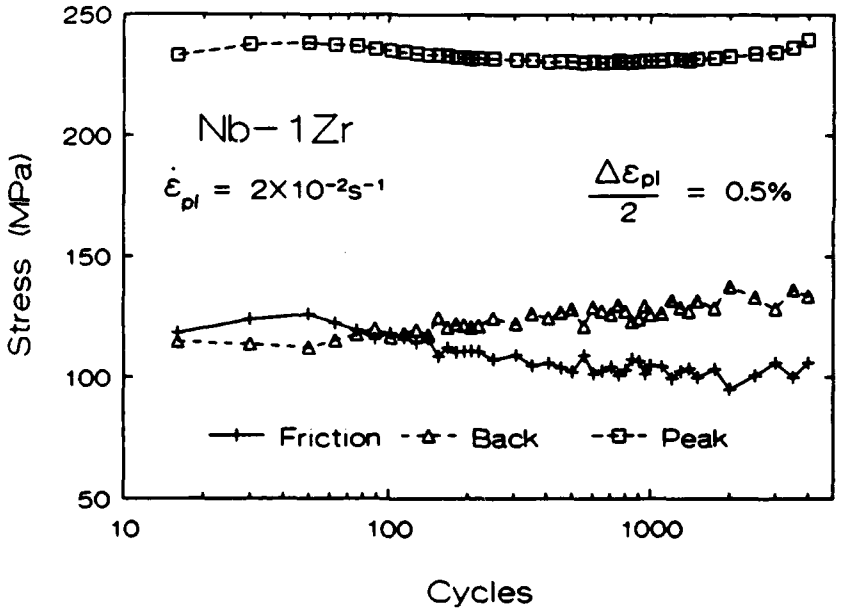

Figure 27: Variation of friction stress, back stress and peak stress with cycles in Nb–1%Zr

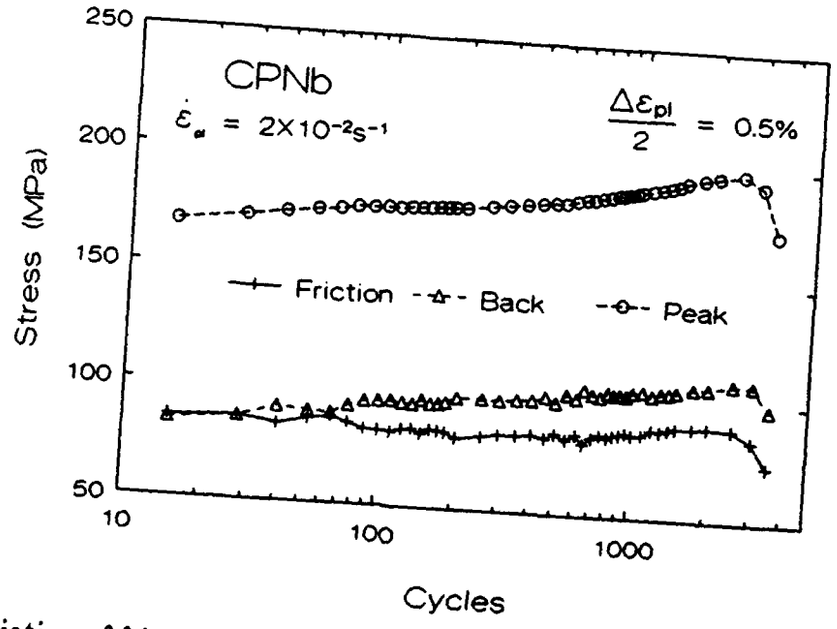

Figure 28: Variation of friction stress, back stress and peak stress with cycles in commercially pure Nb

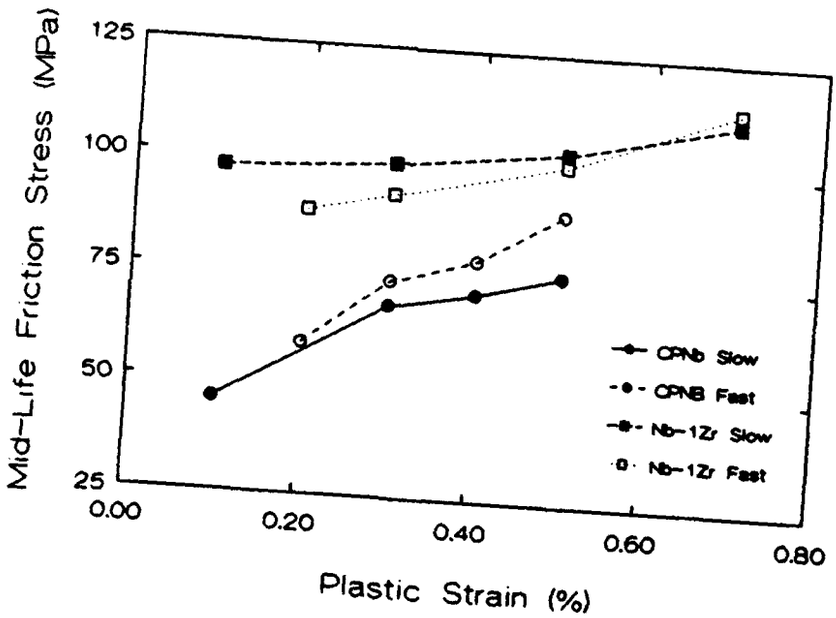

Figure 29: Variation of friction stress with plastic strain amplitude

5.7 References for low cycle fatigue

1. F. Ackermann, H. Mughrabi and A. Seeger: Acta Metall. 1983, vol. 31, pp. 1353-1366
2. M. Anglada and F. Guiu: Philos. Mag. A, 1981, vol. 44, pp. 499-522
3. M. Anglada and F. Guiu: Philos. Mag. A, 1981, vol. 44, pp. 523-541
4. C. English: in Niobium-Proceedings of the International Symposium, H. Stuart, ed., TMS-AIME, Warrendale, PA, 1984, pp. 239-324
5. D.W. Chung and N.S. Stoloff: Metall. Trans. A, 1978, vol. 9, pp. 1387- 1399
6. H. Mughrabi, K. Herz and X. Stark: Int. J. Fract., 1981, vol. 17, pp. 193- 220
7. L.N. Chang, G. Taylor and J.W. Christian: Acta Metall., 1983, vol. 31, pp. 37-42
8. D. Hull and D.J. Bacon: Introduction to Dislocations, 3rd ed., Pergamon Press, Oxford, U.K., 1984, p. 124
9. Metals Handbook, 9th ed., vol. 3, American Society for Metals, Metals Park, Ohio, 1980, p. 333
10. J.W. Martin and L. Edwards: in Micromechanisms of Plasticity and Fracture, Parsons Press, Trinity College, Dublin, 1983, pp. 333-368
11. H. Mughrabi: Scripta Metall., 1979, vol. 13, pp. 479-484
12. H. Mughrabi, K. Herz and F. Ackermann: in Proc. of 4th Int. Conf. on the Strength of Metals and Alloys, Nancy, 1976, pp. 1244-1248
13. H. Mughrabi: in Dislocations and Properties of Real Materials, Institute of Metals, London, 1985, p.244-262
14. H. Mughrabi: in Proc. of 5th Int. Conf. on the Strength of Metals and Alloys, P. Haasen, V. Gerold, and G. Kosterz, eds., Pergamon Press, Oxford, 1980, pp. 1615-1638
15. T. Magnin and J. H. Driver: in Low Cycle Fatigue and Life Prediction, ASTM STP 770, C. Amzallag, B.N. Leis and P. Rabbe, eds., American Society for Testing and Materials, Philadelphia, 1982, pp. 212-226
16. D. Kuhlmann-Wilsdorf and C. Laird: Mater. Sci. Eng., 1979, vol. 37, pp. 111-120

6 CONCLUSIONS

6.1 Conclusions for creep tests

1. RRR niobium, cp Nb–1%Zr and RRR Nb–1%Zr were tested under constant stress creep conditions as well as after stress reduction;

2. The monotonic creep behavior of cp Nb–1%Zr and RRR Nb–1%Zr are qualitatively the same and they show a transient creep behavior similar to dispersion hardened materials. The creep behavior of RRR Nb is typical for a metal class (pure) material;

3. Thorough TEM investigations were done. They showed that only a few particles are present in the as–received condition, too few to explain the transient creep behavior;

4. The model of subgrain coarsening was applied to the investigated alloys and it was possible to explain the primary creep transients on the basis of the coarsening of an inherited fine subgrain structure;

5. The steady state creep rates of all investigated materials could succesfully be described by existing creep models;

6. Stress reduction tests performed on the alloys revealed that the secondary creep transients are similiar to those of pure FCC materials;

7. A plot of the reduced creep rate as a function of the reduced stress showed that similar to FCC materials, in BCC materials two mechanisms with two different stress dependences are acting. The low stress branch (recovery branch) can be attributed to subgrain boundary migration. A plausible explanation of the high stress branch cannot be given at present time. It is assumed that a change from thermally activated dislocation intersection to Peierls mechanism occurs;

8. An increase in creep strength by internally oxidizing could not be achieved in the present work. Investigations clearly showed that an oxidizing treatment weakens the microstructure due to overaging of formed zirconia particles and by decreasing the amount of solute zirconium atoms, which strengthen the material through solid solution hardening.

6.2 Conclusions for low cycle fatigue tests

1. Commercially pure niobium and niobium-1cycle fatigue conditions. Each metal was tested at slow ($2 \cdot 10^{-4}s^{-1}$) and fast ($2 \cdot 10^{-2}s^{-1}$) strain rates. Only cyclic hardening occurred in both metals at each strain rate;

2. The cyclic stresses were always higher in the fast strain rate tests than in the slow strain rate tests at the same plastic strain amplitude. The difference between the fast and slow strain rate cyclic response is greater for commercially pure niobium than for niobium-1%zirconium. This difference is attributed to the fact that the edge and screw dislocation mobilities are more nearly equal in niobium-1%zirconium as a result of the interaction between the edge dislocations and the zirconium substitutional atoms;

3. Both metals have the same fatigue life at equal plastic strain amplitudes. The strain rate had no effect on the cyclic lifetime;

4. The expected behavior for these BCC metals in the low temperature (fast strain rate) regime, where screw dislocation mobility is limited, was observed. Specifically, intergranular cracking occurred and a microplastic plateau was observed in the commercially pure material. A microplastic plateau was not detected at the lower strain rate;

5. The presence of the microplastic plateau and the cyclic stress amplitude of this plateau support the proposal that the limited mobility of screw dislocations in the microplastic plateau is the physical origin of the fatigue limit;

6. The mechanisms of cyclic deformation in polycrystalline niobium are consistent with previously published descriptions of single crystal behavior.

7 PERSONNEL – DEGREES AWARDED

The following personnel are primarily in the work of this program:

Professor Amiya K. Mukherjee, Principal Investigator

Professor Jeffery C. Gibeling, Co – Principal Investigator

Dr. Maximilian A. Biberger, Visiting Assistant Researcher

Dr. Hong Sheng Yang, Postgraduate Researcher

Dr. Koji Tanaka, Visiting Assistant Researcher

Mr. Michael J. Davidson, PhD degree expected in July, 1992

Mr. John M. Meininger, MS degree awarded in September, 1990

Mr. Jorge Robles, Graduate Research Assistant, MS degree expected June, 1992

8 AFOSR SUPPORTED PUBLICATIONS AND PRESENTATIONS

1. CAVITATION AND FRACTURE OF IN9052 AND IN90211 MECHANICALLY ALLOYED ALUMINUM AT HIGH TEMPERATURE,
   T.R. Bieler, L.K. Sadilek, S.F. Meagher and A.K. Mukherjee, in:
   Hot deformation of Aluminium alloys, Ed. T.G. Langdon et al., TMS-AIME, pp. 309 – 318, Warrendale, PA, 1991

2. DEFORMATION MECHANISMS IN TWO MECHANICALLY ALLOYED ALUMINUM ALLOYS AT HIGH HOMOLOGOUS TEMPERATURES,
   T.R. Bieler, S.F Meagher, J.A. Diegel and A.K. Mukherjee, in:
   Hot Deformation of Aluminum Alloys, Ed. T.G. Langdon et al., TMS-AIME, pp. 297 – 308, Warrendale, PA, 1991

3. SUPERPLASTICITY IN METALS, CERAMICS AND INTERMETALLICS,
   A.K. Mukherjee, to be published in Volume 6 in:
   Plastic Deformation and Fracture of Materials, H. Mughrabi, volume editor, in the series "Materials Science and Technology" by VCH Verlagsgesellshaft mbH, Germany

4. STRESS REDUCTION TESTS ON NIOBIUM–1WT%ZR AT 1300 K,
   M. Biberger, M. J. Davidson and A. K. Mukherjee, submitted to Acta Metallurgica

5. CREEP OF NIOBIUM AND SOLID SOLUTION STRENGTHENED NB–1WT%ZR,
M. J. Davidson, M. Biberger and A. K. Mukherjee, submitted to Acta Metallurgica

6. THE ROLE OF MIXED CLIMB PROCESS OF DISLOCATION CREEP OF PARTICLE HARDENED MATRIX,
A.K. Mukherjee, Annual Meeting, Japan Institute of Metals, Sendia, Japan, 1990

7. α - GRAIN SIZE AND β - VOLUME FRACTION ASPECTS OF THE SUPERPLASTICITY OF Ti–6Al–4V,
M. L. Meier and A. K. Mukherjee, Materials Science and Engineering, Vol. A 136, p.71 - 78, 1991

8. SCALING LAW IN SUBSTRUCTURAL CREEP,
A.K. Mukherjee, Oxford University, June 29, 1991

9. STRESS DROP TRANSIENTS REVISITED,
A.K. Mukherjee, Royal Institute of Technology, Stockholm, August 21, 1991

10. HIGH STRAIN RATE SUPERPLASTICITY,
A.K. Mukherjee, Tohoku University, Sendai Japan, September 15, 1991

11. CONSTITUTIVE EQUATIONS FOR STRUCTURAL EVOLUTION IN HIGH STRAIN PLASTICITY,
A.K. Mukherjee, Cornell University, Department of Applied Mechanics, October 20, 1991

12. CREEP AND AGING RESPONSE OF A RAPIDLY SOLIDIFIED Al-Fe-V-Si ALLOY,
R. J. Lewis and J. C. Gibeling, to be published in Scripta Metallurgica et Materialia

13. ELEVATED TEMPERATURE CREEP OF A RAPIDLY SOLIDIFIED Al-Fe-V-Si ALLOY,
R. J. Lewis and J. C. Gibeling, presented at the TMS Annual Meeting, Las Vegas, NV, March 1989

14. CREEP AND AGING RESPONSE OF A RAPIDLY SOLIDIFIED Al-Fe-V-Si ALLOY,
R. J. Lewis and J. C. Gibeling, presented at AeroMat '90, Long Beach, CA, May, 1990

15. LOW CYCLE FATIGUE OF NIOBIUM AND NIOBIUM - 1%ZIRCONIUM ALLOYS,
J. M. Meininger and J. C. Gibeling, submitted to Metallurgical Transactions

16. LOW CYCLE FATIGUE OF NIOBIUM AND NIOBIUM - 1%ZIRCONIUM ALLOYS,
J. M. Meininger and J. C. Gibeling, presented at the TMS Annual Meeting, San Diego, CA, March 1993

A Appendix A

A.1 Manufacturing of niobium and Nb–1%Zr sheet material

The following sketch shows schematically the process of manufacturing cp niobium – and cp Nb–1%Zr sheet material:

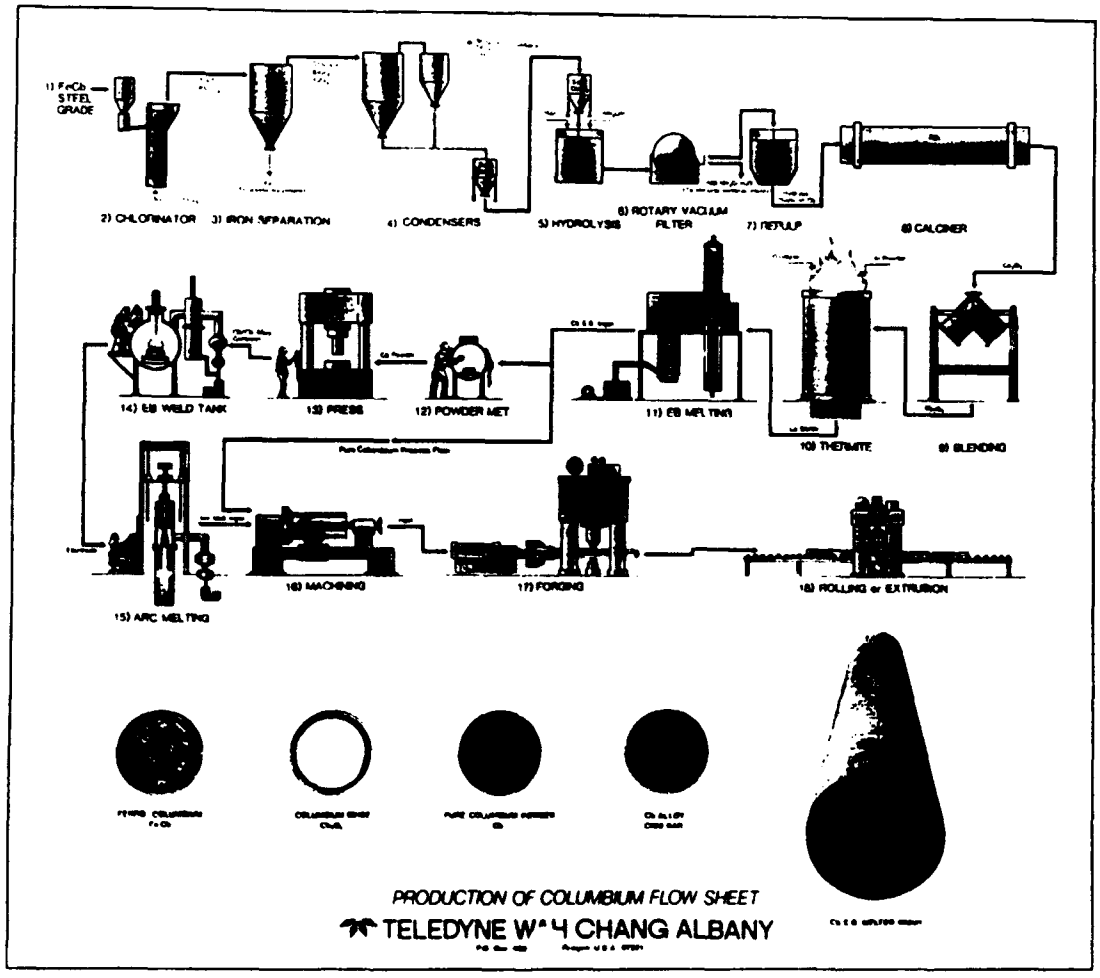

Figure 30: Manufacturing process of cp Nb and Nb-1%Zr

A.2 Chemical composition of the materials used in this work

On the following two pages the chemical composition for RRR niobium and RRR Nb–1%Zr is listed:

Page 1 of 1

TELEDYNE WAH CHANG ALBANY

P O BOX 460
ALBANY OREGON 97321-0130
(503) 926-4211 TWX (510) 906-0973

TO SANDIA NATIONAL LABS
ADDRESS Payment Processing Div. 154
P.O. Box 5800
Albuquerque, NM 87185

ATTENTION OF: Purchasing Agent

IN REGARD TO YOUR
PURCHASE ORDER NO. 90-4346
ITEM NO. 1
DESCRIPTION Niobium RRR Plate-Annealed
DIMENSIONS .030" x 12-3/4" x 24" L
SPECIFICATIONS Per Purchase Order

DATE January 9, 1991
DATE SHIPPED Ref. P.L.#
QUANTITY SHIPPED 1 pc.
WEIGHT SHIPPED 2.8 lbs.
SALES ORDER NO. 5187
HEAT NO. 501293 Nb
PACS NO. 86574

THE TEST REPORT FOLLOWS:

INGOT ANALYSIS IN PPM

Element	1	2	3	4	5
Al:	<20	<20	<20	<20	<20
B:	<1	<1	<1	<1	<1
C:	<30	<30	<30	<30	<30
Ca:	<20	<20	<20	<20	<20
Cd:	<5	<5	<5	<5	<5
Co:	<10	<10	<10	<10	<10
Cr:	<20	<20	<20	<20	<20
Cu:	<40	<40	<40	<40	<40
Fe:	<50	<50	<50	<50	<50
H:	<5	---	<5	---	<5
Hf:	<50	<50	<50	<50	<50
Mg:	<20	<20	<20	<20	<20
Mn:	<20	<20	<20	<20	<20
Mo:	<50	<50	<50	<50	<50
N:	31	---	18	---	17
Ni:	<20	<20	<20	<20	<20
O:	<50R, <50R	---	<50R, <50R	---	<50R, <50R
P:	<30	<30	<30	<30	<30
Pb:	<20	<20	<20	<20	<20
Si:	<50	<50	<50	<50	<50
Sn:	<10	<10	<10	<10	<10
Ta:	790	800	800	790	800
Ti:	<40	<40	<40	<40	<40
V:	<20	<20	<20	<20	<20
W:	33	38	36	<30	34
Zr:	<100	<100	<100	<100	<100

INGOT RESIDUAL RESISTIVITY RATIO TEST RESULTS

Top:	Room temperature - 270	Ice - 263
Bottom:	Room temperature - 261	Ice - 238

Figure 31: Chemical composition of RRR Nb (Teledyne Wah Chang Albany, USA)

TELEDYNE WAH CHANG ALBANY

P.O. [illegible]
ALBANY, [illegible]
(503) [illegible] FAX (503) [illegible]

TO UNIV. OF CALIFORNIA-DAVIS
ADDRESS MECH
1228 Bainer Hall
Davis, CA 95616

ATTENTION OF: Purchasing Agent

IN REGARD TO YOUR
PURCHASE ORDER NO. DT22640
ITEM NO. 1
DESCRIPTION Nb/1% Zr Sheet - Annealed
DIMENSIONS .030" x 12" x 24"
SPECIFICATIONS Per Purchase Order

DATE June 6, 1989
DATE SHIPPED Ref. P.L.# /
QUANTITY SHIPPED 1 pc.
WEIGHT SHIPPED 2.8 lbs.
SALES ORDER NO. 5071
HEAT NO. 531048 Nb1Zr
PACS NO. 74661

THE TEST REPORT FOLLOWS:

INGOT ANALYSIS
COMPOSITION IN PERCENT

Element	1	2	3	4	5
Zr:	0.93	0.92	0.89	0.88	0.88
Nb		B A L A N C E			

MAXIMUM IMPURITIES IN PPM

Al:	20	21	<20	20	23
B:	<1	<1	<1	<1	<1
C:	<30	<30	<30	<30	30
Cr:	<20	<20	<20	<20	<20
Cu:	<10	<10	<10	<10	<10
Fe:	<50	<50	<50	<50	<50
H:	<5	---	---	---	5
Hf:	<50	<50	<50	<50	<50
Mo:	<50	<50	<50	<50R	<50
Mo:				55R	
N:	10	---	---	---	17
Ni:	<20	<20	<20	<20	<20
O:	110	---	---	---	<50
Si:	<50	<50	<50	<50	<50
Sn:	<10	<10	<10	<10	<10
Ta:	1640	1670	1710	1710	1680
Ti:	<40R	<40R	<40R	<40	<40R
Ti:	<40R	<40R	<40R		<40R
V:	<20	<20	<20	<20	<20
W:	46	42	56	56	64

MATERIAL CERTIFIED BY Jill Schaefer 6/5/89
WC
Jill Schaefer
Quality Assurance Dept.

A1.04.01.17 P1-1
C1.08.09.21

Figure 32: Chemical composition of RRR Nb–1%Zr (Teledyne Wah Chang Albany, USA)

The following list shows the procedures for the preparation of TEM specimens. The guidelines were provided from Teledyne Wah Chang, Albany. We gratefully acknowledge their support.

1. Grind

   1.1 120 grit.
   1.2 400 grit.
   1.3 #0, #00, #000 alumina paper.

2. Rough Polish

   2.1 Silk cloth over metcloth lap at 1150 rpm.
   2.2 Slurry composed of 10 ml 20% chromic acid, 8-10 g Linde C alumina (1.0μ), and 150 ml H_2O (see comments).

3. Intermediate Polish

   3.1 Microcloth lap at 1150 rpm.
   3.2 Slurry composed of 5 g Linde B alumina (0.05μ) and 150 ml H_2O.
   3.3 Base solution composed of 10 g $K_4Fe(CN)_6$, 10 g NaOH, and 100 ml H_2O (see comments).

4. Final Polish

   4.1 Chemomet lap at 1150 rpm.
   4.2 Mastermet solution.
   4.3 Base solution (small amount) given in 3.3.

5. Etch

   Etch with solution composed of 10 ml lactic, 10 ml HNO_3, 10 ml HF, and 10 ml H_2O_2 (see comments).

Comments of Procedure

During the intermediate polishing approximately 3 to 5 ml of the base solution given in paragraph 3.3 is added to the lap to aid in the removal of flowed metal and scratches. The specimen should be swab etched with the solution given in paragraph 5 prior to and following the rough polish step. The final etch is performed by immersion etching with the solution given in paragraph 5.

Procedure used at TWCA, Albany, Oregon
September 1, 1990.

Figure 33: TEM sample preparation provided by: Teledyne Wah Chang Albany, USA

Element	cp Nb	Nb–1%Zr
Al	<20	<20
B	—	<1
C	<30	48
Cr	<20	<20
Cu	<40	<40
Fe	<50	<50
H	<5	<5
Hf	<50	<50
Mo	<50	<50
N	23	42
Ni	<20	<20
O	<50	<50
P	<25	—
Si	<50	<50
Sn	<10	<10
Ta	2013	1422
Ti	<50	<50
V	<20	<20
W	80	78
Zr	<100	9200

Table 2: Chemical Analysis of Materials used in the Fatigue Tests: Ingot Analysis (composition in ppm)